



Review

Recent Advances in the Application of Nanozymes in Amperometric Sensors: A Review

Liu Tong^{1,2}, Lina Wu², Enben Su², Yan Li^{1,*}  and Ning Gu^{1,3,*} 

¹ State Key Laboratory of Bioelectronics, Jiangsu Key Laboratory for Biomaterials and Devices, School of Biological Science and Medical Engineering, Southeast University, Nanjing 210009, China

² Getein Biotechnology Co., Ltd., Nanjing 211505, China

³ Medical School, Nanjing University, Nanjing 210093, China

* Correspondence: liyan@seu.edu.cn (Y.L.); guning@nju.edu.cn (N.G.)

Abstract: Amperometric sensors evaluate current changes that occur as a result of redox reactions under constant applied potential. These changes in current intensity are stoichiometrically related to the concentration of analytes. Owing to their unique features, such as fast reaction velocity, high specificity, abundant existence in nature, and feasibility to be immobilized, enzymes are widely used by researchers to improve the performance of amperometric sensors. Unfortunately, natural enzymes have intrinsic disadvantages due to their protein structures. To overcome these proteinic drawbacks, scientists have developed nanozymes, which are nanomaterials with enzymatic properties. As the result of significant advances in materialogy and analytical science, great progress has been achieved in the development of nanozyme-based amperometric sensors with outstanding performance. To highlight achievements made in recent years, we first summarize the development directions of nanozyme-based amperometric sensors. Then, H₂O₂ sensors, glucose sensors, sensors combining natural enzymes with nanozymes, and sensors targeting untraditional specific targets will be introduced in detail. Finally, the current challenges regarding the nanozymes utilized in amperometric sensors are discussed and future research directions in this area are suggested.

Keywords: amperometric sensors; H₂O₂ sensor; glucose sensor; nanozyme; minireview



Citation: Tong, L.; Wu, L.; Su, E.; Li, Y.; Gu, N. Recent Advances in the Application of Nanozymes in Amperometric Sensors: A Review. *Chemosensors* **2023**, *11*, 233. <https://doi.org/10.3390/chemosensors11040233>

Academic Editor: Alina Vasilescu

Received: 28 February 2023

Revised: 31 March 2023

Accepted: 7 April 2023

Published: 9 April 2023



Copyright: © 2023 by the authors. Licensee MDPI, Basel, Switzerland. This article is an open access article distributed under the terms and conditions of the Creative Commons Attribution (CC BY) license (<https://creativecommons.org/licenses/by/4.0/>).

1. Introduction

Electrochemical sensors have an irreplaceable position in the field of analysis for their outstanding advantages, such as great sensitivity, simple miniaturization for personal use, diverse electrochemical methodologies targeting different analytes, etc. [1–4]. Amperometry, as an important subclass of electrochemical methods, is commonly paid the most attention for its adaptability in biosensing various analytes [5–7]. Blood glucose test strips, the most widely used commercial point-of-care product in clinical practice, are mainly based on amperometry [8–10]. In amperometry, current changes generated by redox reactions are monitored by applying a constant potential to the working electrode [2]. The current intensity corresponds to the electroactive species content in the sample. Moreover, the oxidation or reduction potential used for detection is characteristic of the analyte, thus offering additional selectivity.

Amperometric methods mainly focus on assaying whether substances have redox properties [11] or are used in situations where redox reactions occur when non-redox targets, transferred to stoichiometric redox intermediates, are then detected by an electrode. As shown in Figure 1, in the first scenario, the direct transfer of electrons occurred between the redox target and electrode surface due to a constantly applied external potential. The matrix effects of natural samples always lead to overpotential on the sensor's surface; therefore, higher or lower external potentials have to be applied to initiate electron transfer between the redox targets and the electrode [12]. Overapplied potential will introduce unspecific redox reactions in complex natural samples. To solve this problem, enzymes are

commonly used as specific electron transporter mediators to reduce the initiated potential or as electron mediators for their high specificity and fast reaction velocities, in turn, reducing undesired background activity while enhancing the specific current response [13]. In the second scenario, non-redox targets cannot be directly oxidized or reduced on the electrode. In this case, some targets can be treated as substrates of their related enzymes to produce stoichiometric intermediates with redox properties [14].

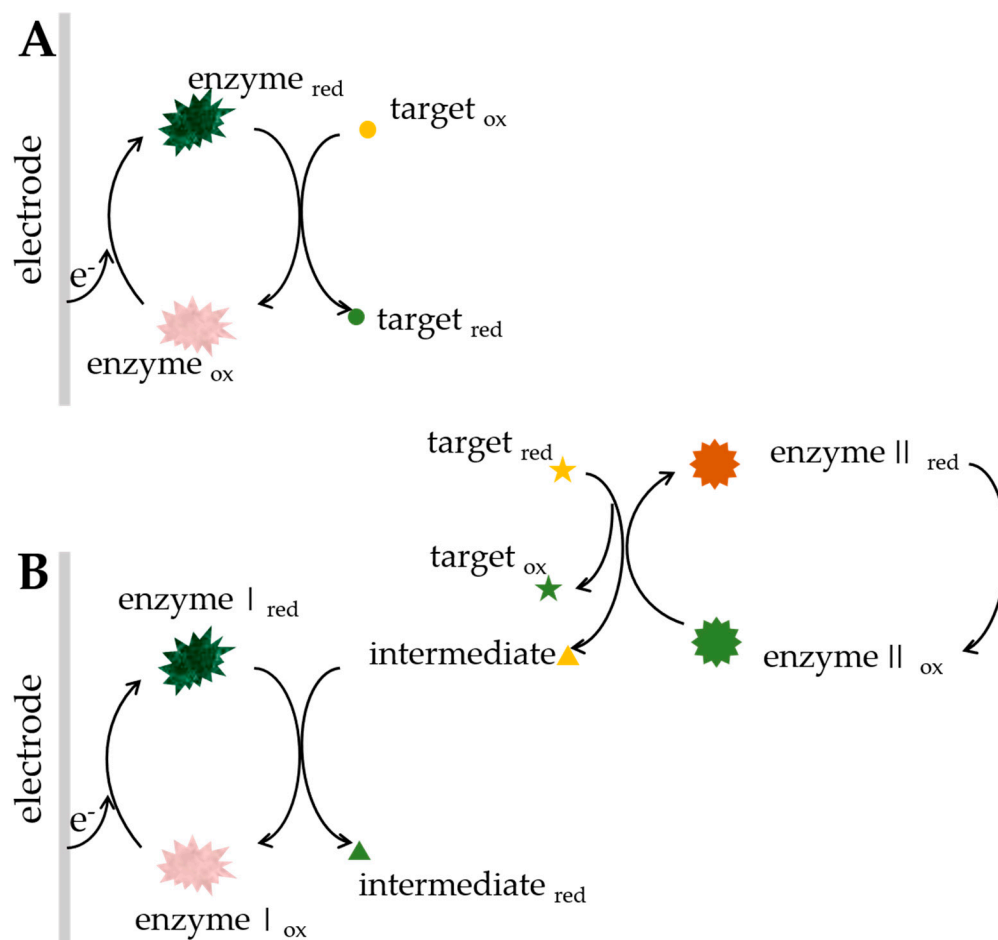


Figure 1. (A) Scheme of the sensors' target substances that have redox properties. (B) Scheme of sensors where redox reactions happened when non-redox targets were transferred to redox intermediates and then detected by the electrode.

As we can see, enzymes play a key role in amperometry. They give the amperometric sensors more specificity and practicability. Unfortunately, naturally derived enzymes have intrinsic shortcomings, which greatly limit their application. Nanozymes, the generic term for nanoscale materials with enzyme-like properties, intrinsically possess many advantages over their natural counterparts, which are mostly globular proteins (except for some RNA ribozymes) [15,16]. Firstly, nanozymes are easy to handle in the production process as they are commonly stored in liquid solutions, while natural enzymes are manufactured in the form of lyophilized powder, which has to be weighed quantitatively and then prepared as solutions before use and easily absorbs moisture. Secondly, nanozymes can resist high-temperature conditions, while the prepared natural enzyme solutions can only be stored for a few days at room temperature. Thirdly, nanozymes can be synthesized from basic chemical materials, which contributes to their shorter manufacturing process and cheaper production cost. Fourthly, the direct modification of natural enzymes on electrodes may somehow change their steric structures, thus decreasing enzymatic activity; the nanozymes' structures are generally more rigid, which can better preserve their electrocatalysis in

amperometric sensors. Last, but not least, considering enzymes are themselves insulated proteins, the electron-transfer efficiency in protein-modified sensors can be lower than sensors modified with nanozymes, which are composed of highly conductive materials. All of these properties have prompted scientists and engineers to utilize nanozymes instead of natural enzymes for enzymatic sensors.

In the last five years, researchers have made great progress in developing nanozyme-based amperometric sensors with good performance. In addition to using new nanozymes, a new trend has begun to combine the traits of several nanomaterials together to improve the performance of amperometric sensors. Among the objects detected by amperometry, H_2O_2 is the most common substance detected for its redox activity; another reason for this is that H_2O_2 is the final product of many biochemical reactions. Glucose is another common amperometric target because of its crucial role in the diagnosis and control of diabetes.

Our review aims to highlight the progress of nanozyme-based amperometric sensors in the last five years. We will then describe the amperometric nanozymatic sensors targeting H_2O_2 and glucose. Then, sensors combining natural enzymes with nanozymes are discussed. Next, sensors targeting other substances are introduced. Finally, we discuss the challenges faced by nanozyme-based amperometric sensors and propose future directions for research.

2. Nanozymes Used in Amperometric Sensors

2.1. Nanomaterials with POD-Like or Oxidase-Like Properties

Generally, nanozymes can be divided into oxidoreductase and hydrolase [17]. Hydrolase does not directly participate in the electron transfer process. In this section, we detail two members of the oxidoreductase family, peroxidase (POD) and oxidase, for their wide application in catalytic redox reactions involving enzymes and amperometric sensors.

H_2O_2 amperometric sensors are widely used in environmental monitoring and the food industry since H_2O_2 itself has redox activity. Some interfering substances in the human body's fluids oxidize at similar potentials of H_2O_2 , thus significantly affecting the specificity of the H_2O_2 sensor. Therefore, it is highly desirable to develop peroxidase (POD)-like nanozymes with good selectivity, high electrocatalytic activity, and excellent conductivity.

Since Yan et al. first discovered in 2007 that Fe_3O_4 nanoparticles (NPs) possess POD-like activity [18], diversified nanomaterials have been proven to be in possession of POD-like activities. Some of the nanomaterials' enzyme-like mechanisms have already been uncovered. For example, our group successfully elucidated the nanozymatic mechanisms of Prussian blue nanoparticles (PB NPs) and Fe_3O_4 NPs (Figure 2) [19,20].

As listed by Qu et al., 139 nanomaterials with POD activity had been reported before 2019 [17]. From then on, the development of nanozymes became more and more rapid. Generally, POD-like nanozymes are constructed using nanomaterials based on various nanostructured metals or alloys, metal oxides or their mixtures, diversified carbon materials, metal-organic frameworks (MOFs), or a combination of the above materials. To clarify the types of nanozymes according to the metal elements involved in the constitution of most nanozymes [21], we classified some nanomaterials with POD-like properties that have been developed since 2020 into: nanomaterials containing one metal element (e.g., cobalt oxide (Co_3O_4) nanodisk, tungsten disulfide (WS_2) nanosheets, gold nanoclusters, and rodlike TiO_{1+x}) [22–25]; nanomaterials containing bimetallic elements (e.g., Fe_3O_4 - TiO_2 /graphene nanocomposites, $Co_3V_2O_8/Co_3O_4$ nanowires, 0D/2D Au_xPd_{100-x} nanocomposites, Pd-Ir core-shell nanoparticles [26–29]; nanomaterials containing multiple metal elements (e.g., $Au@PtRu$) [30]; non-metal-based nanomaterials (e.g., nitrogen-doped graphene, histidine-functionalized graphene quantum dots/hemin complex) [31,32]; MOF-based nanomaterials (e.g., 2D Cu-TCPP(Fe) MOFs and quasi-MOF_{ce0.5}) [33,34].

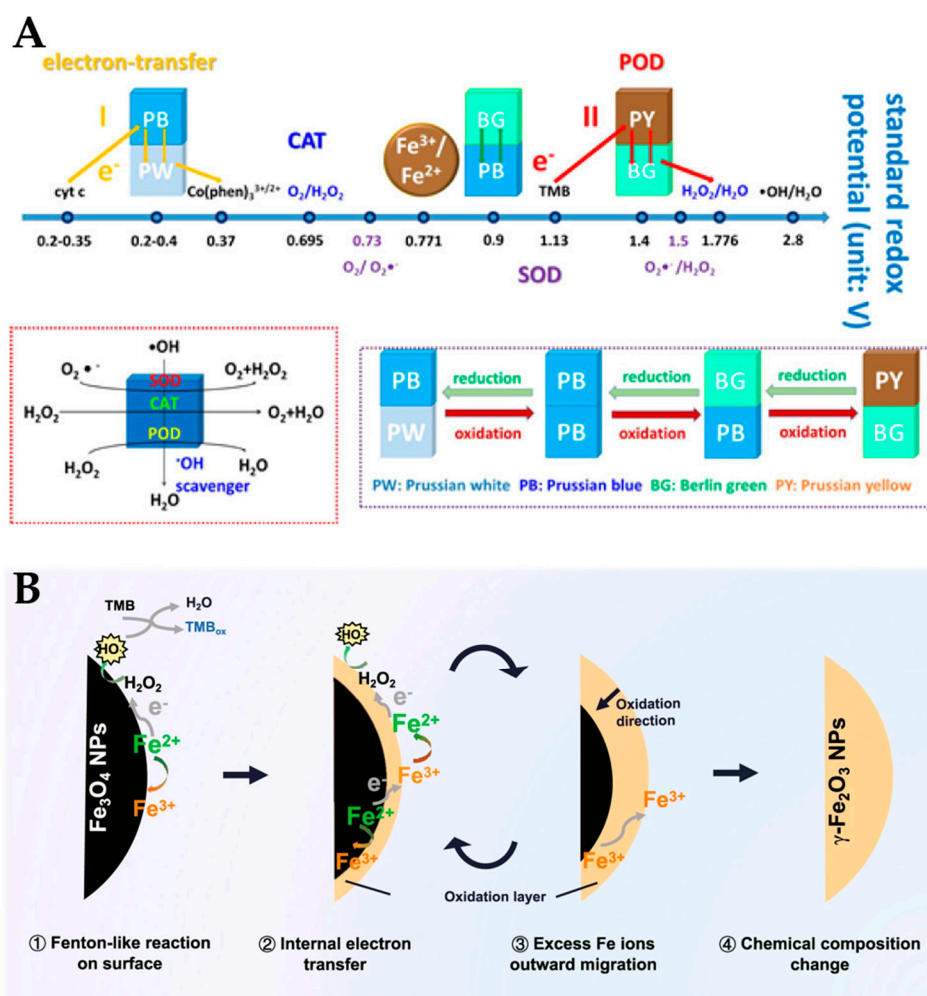


Figure 2. (A) The mechanism of the multienzyme-like property of PB NPs, based on standard redox potentials [19]; (B) the mechanism of the POD-like property of Fe₃O₄ NPs [20]. Copyright: American Chemical Society and Nature Publishing Group.

The rapid detection of glucose concentration levels is essential in diabetes diagnostics and monitoring. The most common technique for glucose assay is the glucose oxidase (GOX)-based amperometric method. Due to the intrinsic shortcomings of natural GOX, great attention has been paid by scientists to developing glucose biosensors without enzymes. In 2004, Comotti et al. first discovered that “naked” AuNPs exhibited GOX-like activity in the presence of O₂ [35]. In recent years, various oxidase mimics have been developed, such as Fe-N-C, Cu₂O-CDs-Cu nanospheres (3000 nm), MoO₃ nanoparticles (2–4 nm), CeO₂@MnO₂ core-shell hollow nanospheres, Cu-Ag NPs, glutathione-Cu/Cu₂O nanoparticles, and Co-N_x sites on porous carbon (Co-N_x/PC) [36–42].

The maximal reaction rate (V_{max}) indicates the reactivity of nanozymes at fixed concentrations when the substrates are saturated [43]. The Michaelis constant (K_m), the concentration of substrates at half of V_{max} , is an indicator of an enzyme’s affinity for its substrate. A lower K_m value means that there is a stronger affinity between the enzymes and their substrates. K_{cat} indicates the maximum number of substrates transformed into the product by every enzyme per second [44]. The above parameters can be used to evaluate the catalytic activity of nanozymes from different viewpoints. Generally, a POD-like nanozyme has a higher K_m for H₂O₂, while the K_{cat} value is then higher than that of the natural enzyme [18]. This may be ascribed to the fact that nanozymes have more active sites; however, the specificity of the nanozymes is unsatisfactory due to their having fewer substrate binding sites [45]. For oxidase-like nanomaterials, most of their K_m values are

lower than those of natural enzymes, meaning that the nanozymes have a higher affinity toward substrates [45].

Many factors can influence the activities of nanozymes; among them, the effects of size are the most fundamental. In different nanozymes, the size effects can also follow different rules. Just as with Fe_3O_4 NPs, the smaller the size (30–300 nm), the greater the POD-like activity [18]. However, in the case of Pd-Ir nanoparticles, the POD-like activities increase with a particle size within the range of 3.3–9.8 nm [29]. These results demonstrated that the size effect is an essential factor that influences the nanozymes' activities; no fixed rules can be applied indiscriminately. Designers must take the size effect into consideration when designing nanozymes in practice.

2.2. Synthesis and Characterization of Representative Nanozymes Used in Amperometric Sensors

When constructing amperometric sensors, the sensors' performance is not only influenced by the activities of nanozymes but also, firstly, which nanozymes retain their catalytic activities when they are assembled on the electrode; secondly, the transfer of electrons from the nanozymes' surface to the electrode surface should not be retarded by immobilized systems.

Scientists constantly endeavor to promote the performance of nanozymatic sensors. They discovered that by combining the specificities of different nanomaterials, the resulting composite materials can overcome some of the shortcomings of single nanoparticles during their application, for example, the agglomeration of nanozymes or obstruction of electron transfer by adhesive agent, thus improving the performance of nanozymatic amperometric sensors (Figure 3). These nanozymatic composites contained materials that acted as a support while others offered enzymatic activities. Support materials can fulfill multiple functions: as templates to grow other nanomaterials; as inhibitors to prevent smaller nanoparticles offering enzymatic activity from aggregating; and as catalytic activity enhancers via synergetic effects.

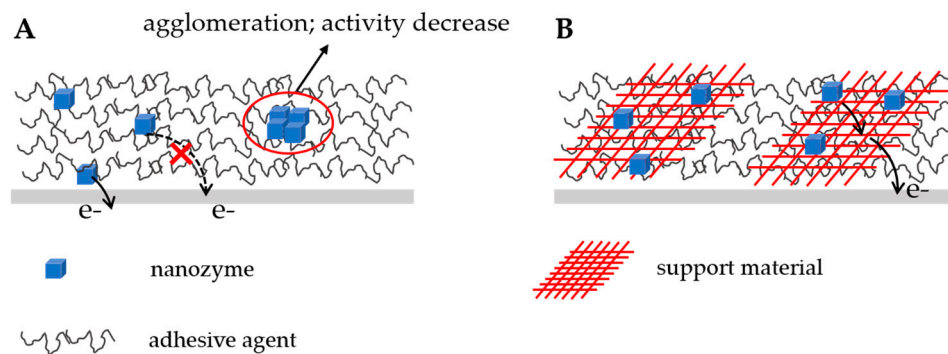


Figure 3. (A) Scheme of a traditional nanozymatic sensor. (B) Scheme of a support material–nanozyme composite sensor.

Two typical routes can be followed to synthesize nanocomposites containing support materials and smaller nanozyme units. One route is that the nanozyme units are grown in situ on the surface of the support materials (Figure 4A). A typical ML_x^- may be PtCl_6^- or AuCl_4^- . Reductive agents may be NaBH_4 or sodium citrate, or any other agents that can reduce the corresponding metal ions. The other route is that the nanozyme units are previously prepared (Figure 4B). The support materials are first activated using coupling agents to graft functional groups to their surface. The pre-prepared nanozyme units are then added to the solution to be assembled on the supports. It must be noted that ultrasonic conditions are essential during the synthesis process for keeping the nanomaterials from aggregation. The centrifugal cleaning process should be conducted several times, with different solvents if necessary, to separate the superfluous unreacted matter in the previous steps and the purified final products in the last step.

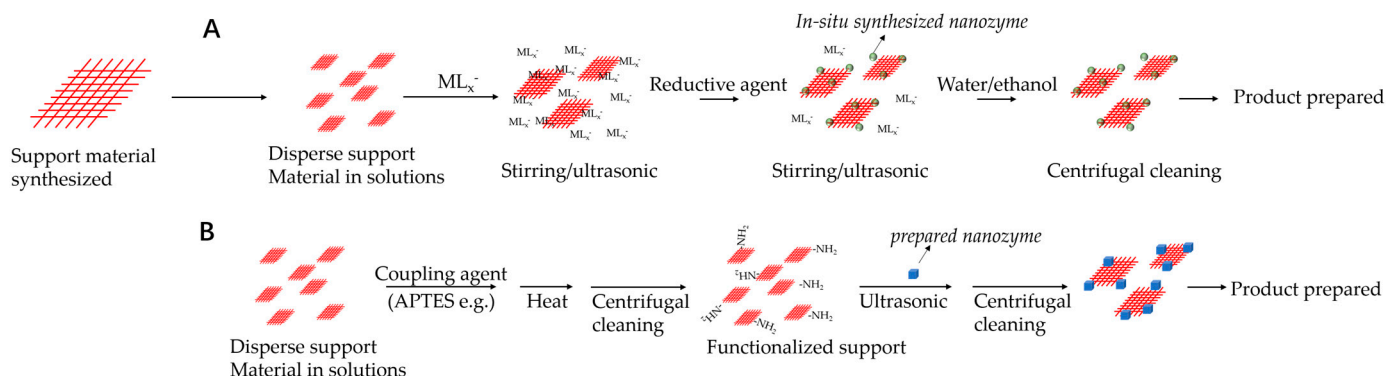


Figure 4. Typical routes to synthesis nanocomposites containing support materials and smaller nanozyme units: (A) the nanozyme units are grown in situ on the surface of the support materials; (B) the nanozyme units are pre-prepared.

The typical method for constructing a nanozyme-based amperometric sensor is as follows. First, the nanozymes are dispersed well in a solution. Generally, the solutions may be Nafion solution, PVP solution, or merely deionized water (DI) water. Nafion and PVP are used as filmogens to better immobilize the nanozymes on the electrode and to further improve the sensor's stability. The solvent is generally DI water, but ethanol, isopropanol, or their mixtures can also be used if necessary. Ultrasonic can be used to disperse the nanozymes well if needed. Second, the nanozymes solution is drop-cast on the electrode surface to dry at room temperature. After it is totally dried on the electrode, a classical nanozyme-based amperometric sensor has been constructed.

The characterization of prepared nanocomposites with enzyme-like properties is essential for researchers to source important information, such as elemental composition, crystal forms, morphology, surface properties, bonding states within materials, and so on. This information can be used not only to explain the properties of prepared materials but can also be used to construct theoretical models to inform the future design of nanozymes. We have listed some of the most frequently used characterization methods in Table 1. One should know that all characterized methods in the laboratory can be used if necessary.

Table 1. Commonly used characterization methods in developing nanozyme-based amperometric sensors.

Methods	Purpose
EDX (energy-dispersive X-ray spectroscopy)	Elemental composition
XRD (X-ray powder diffraction)	Crystalline structure and phase information
FT-IR	Confirming the existence of covalent bonds, and the recognition of functional groups
SAED (selected area electron diffraction)	Crystal structure
TEM	Morphology
SEM	Surface properties and morphology
UV-VIS	Confirming the existence of covalent bonds
Cyclic voltammetry	Electrocatalytic activity
XPS (X-ray photoelectron spectroscopy)	Surface chemical composition and the valence state of elements

3. Applications of Nanozymes in Amperometric Sensors

3.1. Sensors Targeting the Detection of H_2O_2

The oxidation/reduction of H_2O_2 -driven electron transfer on the electrode generates a current depending on the concentration of H_2O_2 [46]. To clarify recent progress in the field, we will split the discussion into sensors for the oxidation and reduction of H_2O_2 .

3.1.1. Sensors for the Reduction of H₂O₂

Nanomaterials containing one metal element. Mesoporous silica microspheres (MSMs) form a classical porous nanomaterial that is often used as a template in nanocomposite preparation. They have a regular array of tunable-sized pores, which provide a high surface area [47,48]. Pd NPs are a form of metal NP that has POD-like activity. However, most of the amperometric sensors that utilize Pd NPs as POD mimics nowadays lack sufficient sensitivity to detect the ultra-low H₂O₂ in cell levels [49,50]. Rupali et al. assembled Pd NPs with sulfonic acid functionalized MSM. The sizes of the Pd NPs range from 2 to 22 nm, with a mean size of 8.9 nm, while the diameter of MSMs ranges from 300 to 400 nm. After being dispersed in a PVA solution, the obtained nanocomposite Pd@SO₃H-MSM was then dried on GCE to construct an amperometric H₂O₂ sensor (Figure 5) [51]. The limit of detection (LOD) of the obtained sensor was 0.014 μM, which is low enough to detect H₂O₂ in cells. The sensor has good stability and can be used after 30 days, with good reproducibility (RSD = 2.6%) (Table 2). It also responds quickly to H₂O₂, yielding a steady signal that can be attained in only 2 s, which is very beneficial for practical applications.

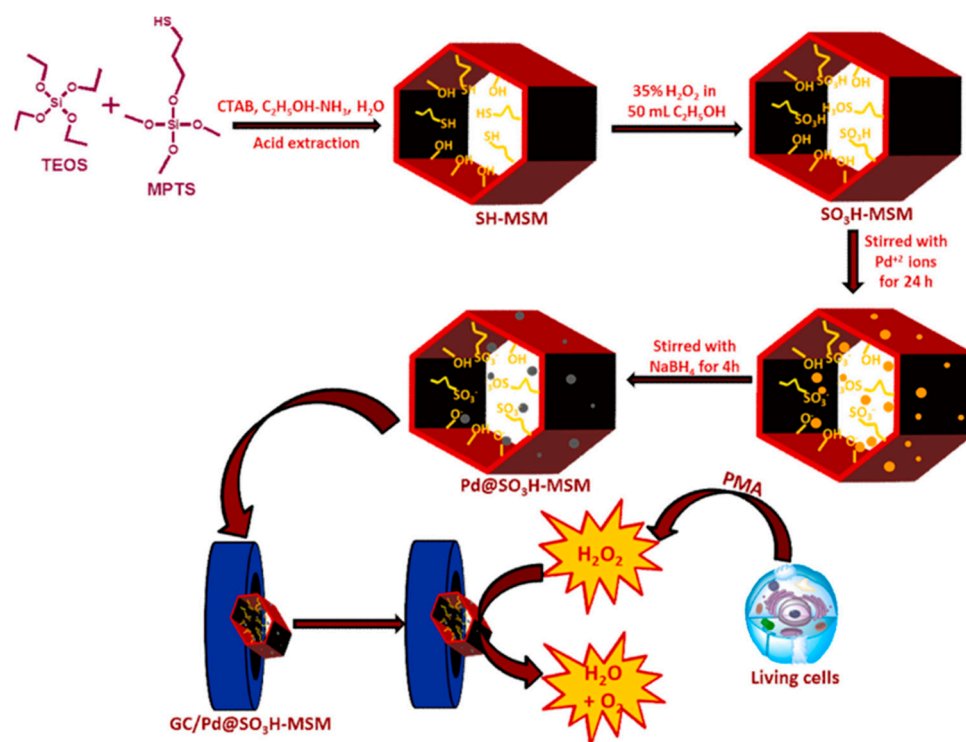


Figure 5. Scheme of a Pd@SO₃H-MSM-modified H₂O₂ sensor [51]. Copyright: Elsevier B.V.

Nanomaterials containing bimetallic elements. Molybdenum carbide (Mo₂C) has been researched in the context of detecting H₂O₂ for its POD-like activity within a wide pH range [52]. Doping Mo₂C with metal that has high conductivity can enlarge the active surface area and conductivity, which further enhances its POD-like activity [53]. Li et al. incorporated the metal Ag into Mo₂C material since Ag has the highest electrical conductivity of metals and good biocompatibility. Via in situ calcination in a N₂/H₂ atmosphere using the single-stage method, prepared coral-like Ag-Mo₂C/C was dispersed in a Nafion solution and then dried on GCE for the electrocatalytic reduction of H₂O₂ [54]. The incorporation of Ag causes shrinkage of the Mo₂C lattice. This interaction tunes the electronic state of the Mo active sites and strengthens their combination with unstable intermediate OH_(ad) during the H₂O₂ reduction process, thus promoting the cleavage of the O-O bond (H₂O₂ + e⁻ → OH_(ad) + OH⁻) and further improving the sensor's response. The sensor has high sensitivity (466.2 μA mM⁻¹ cm⁻²), good stability (the response after 1 month is nearly identical to the initial response), and acceptable reproducibility (RSD

= 2.25%) (Table 2). When H_2O_2 is added, 90% of the steady signal is achieved in only 1.2 s, which is the fastest result from all the nanozyme-based H_2O_2 sensors we have found in recent years. Jesila et al. synthesized silver molybdate (Ag_2MoO_4) nanowires using co-precipitation, assisted with ultra-sonication methods; the prepared nanowires were then used as electrode modification materials to electrochemically reduce H_2O_2 , after which an ultralow LOD (5.42 nM) was achieved (Table 2) [55]. In their study, the nanomaterial was dispersed in water, then dried on GCE. Nevertheless, the sensor had good stability. The response barely changed after storage at 4 °C for 30 days. When H_2O_2 was added, 95.2% of the steady signal could be attained in 4 s. AgNPs have good POD-like activity but easily aggregate. To overcome the severe agglomeration of AgNPs on electrodes, Zhu et al. deposited AgNPs on N-doped Ti_3C_2 to detect H_2O_2 [56]. The hierarchical Ti_3C_2 has a wide size range between 100 nm and 3 μm . When constructing amperometric sensors, the Ag/N- Ti_3C_2 is dispersed in ethanol and then dried on GCE. The resulting sensor has a sensitivity of $552.62 \mu\text{A mM}^{-1} \text{cm}^{-2}$ and good reproducibility (RSD = 3.1%) (Table 2).

Nano Au and Pt alloy microspheres that are decorated with reduced graphene oxide (RGO/nAPAMs) have excellent electrocatalytic activity in terms of reduction toward H_2O_2 at 80 mV (Figure 6) [57]. In this study, Pt and Au were alloyed and distributed on graphene with a size of about 10 nm. Prepared RGO/nAPAMs were dispersed in water before being dried on GCE. The outstanding H_2O_2 sensing performance (sensitivity: $1117.0 \mu\text{A mM}^{-1} \text{cm}^{-2}$) can be attributed mainly to the electro-catalytic property of Pt nanoparticles. Combining them with gold nanoparticles further enhanced their POD-like property. This activity-enhancing effect could be ascribed to the synergistic work between Pt and Au nanoparticles and RGO. The sensor maintains 92.2% of its initial response after 1 month, which is indicative of good stability. This reproducibility is also good for RSD, which is 3.2% (Table 2). Liu and his coworkers synthesized a POD-like nanocomposite consisting of Pt nanoparticles and Au nanoparticles on silica nanorods, using self-assembling methods to achieve the electrocatalytic reduction of H_2O_2 . Au NPs are nanospheres of about 4 nm in diameter, while the Pt NPs are of about 2–3 nm in width and 3–7 nm in length [58]. Interestingly, the authors found that sensors without support materials showed better electrocatalytic activity than those sensors comprising Au/Pt nanoparticles dispersed on a silica support. When H_2O_2 was added, 95% of steady current could be attained in 5 s. This unexpected result can be ascribed to the poor conductivity of silica nanorods in the nanostructures, thus delaying the electrons generated from the catalytic redox reaction of H_2O_2 transfer to the electrode surface. The study demonstrated that the conductivity of supported materials has a great effect on the performance of amperometric sensors; thus, conductivity needs to be considered when choosing support materials.

Nanomaterials containing multiple metal elements. Dai et al. developed $\text{AuPd@Fe}_x\text{O}_y$ nanoparticles as a nanozyme to detect H_2O_2 [59]. The $\text{AuPd@Fe}_x\text{O}_y$ NPs are 52.1 ± 6.1 nm in diameter. The Au and Pd are concentrated at the center of the nanocomposite. The synthesized nanomaterial was first dispersed in ethanol/Nafion and then dried onto a GCE. In amperometry, the sensitivity of an $\text{AuPd@Fe}_x\text{O}_y$ -based sensor is $120.7 \mu\text{A mM}^{-1} \text{cm}^{-2}$. $\text{AuPd@Fe}_x\text{O}_y/\text{GCE}$ sensors have very good reproducibility since the RSD is only 0.63%. They retain over 95% of their initial response after storage at room temperature for 20 days, which is indicative of very good stability (Table 2).

MOF-based nanomaterials. MOFs represent a novel material emerging in developing amperometric sensors due to their unique characteristics. Traditionally, MOFs have an interconnected tridimensional (3D) structure. The properties of the 3D structure will resist active matter transferring into it, thereby diminishing the POD-like properties of MOF-based nanozymes [60,61]. To circumvent this shortcoming, Huang et al. decorated ~3 nm AuNPs on 2D conductive MOF nanosheets (C-MOF (NSs)) to detect H_2O_2 in living cells [62]. Compared with 3D MOF, the 2D materials exposed more electroactive sites during the electro-transfer process. The planar structure greatly enhanced the material's conductivity and facilitated matter diffusion on the electrode [63,64]. The 2D C-MOF NSs not only provided good charge mobility but also offered exposed active sites to decorated AuNPs.

Using Cu-HHTP-NSs as model 2D C-MOF NSs to modify the electrode, the prepared sensor can achieve 95% of a steady current in 3 s while achieving a sensitivity of $188.1 \mu\text{A mM}^{-1} \text{cm}^{-2}$. Besides this, the sensor maintains 93% of its response after 4 weeks, showing good stability and good reproducibility, with a low RSD (3.1%) (Table 2).

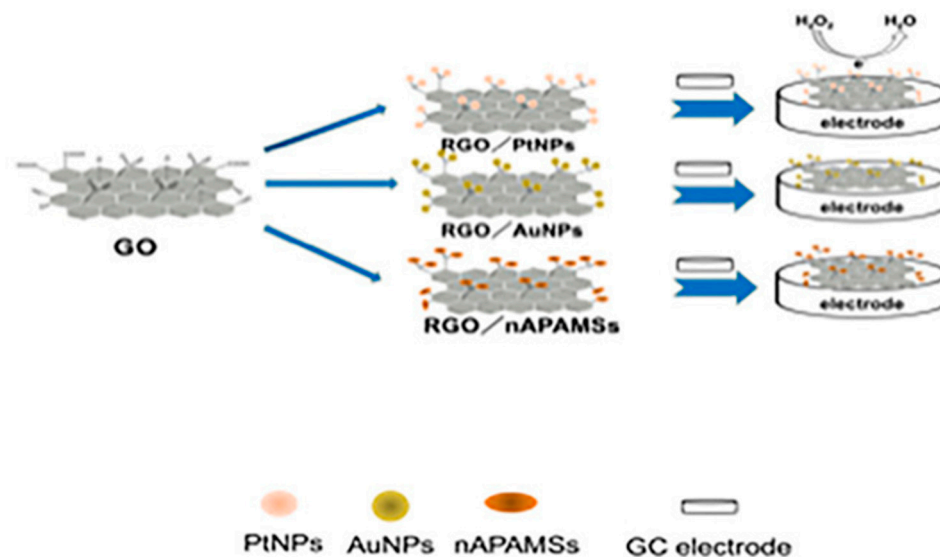


Figure 6. Scheme of an RGO/nAPAMs fabricated H₂O₂ sensor [57]. Copyright: American Chemical Society.

ZIF-67 is a form of MOF porous crystalline material consisting of cobalt as the metal joint and 2-methylimidazole as the ligands [65]. It has a tetrahedral skeleton with good stability in an air atmosphere, neutral pH, and strong alkaline solutions, thus making it a hopeful prospect as a precursor to synthesize porous nanocomposites. By the calcination of ZIF-67 at 600 °C, Wu et al. obtained nitrogen-doped mesoporous carbon composites embedded with Co NPs (0.2 nm) (Co-N-C), which possess a rhombic dodecahedral morphology [66]. The prepared Co-N-C nanocomposite has good conductivity while maintaining the porous structure of ZIF-67 (600 nm), which bestows a large surface area and enhanced electrochemical properties in terms of H₂O₂ reduction. After being dispersed in Nafion/water/isopropanol solution and then dried on a rotating disk electrode, an amperometric sensor was obtained. The resulting sensor can produce a steady current in 6 s. Moreover, it shows very good stability, for it maintains a 92.7% response after storage for 60 days, and outstanding reproducibility for 1.78% RSD (Table 2). Lu et al. prepared a nanozymatic-based H₂O₂ sensor containing gold nanoflowers (AuNFs), Fe₃O₄, ZIF-8, and MoS₂ together (Figure 7) [67]. Fe₃O₄ NPs are well known for their classical POD-like activity. ZIF-8 is another form of MOF porous material with a large surface area that utilizes Zn as a metal joint [68,69]. The hybrid nanomaterial Fe₃O₄@ZIF-8 is spherical in shape, with a diameter of 190 nm. It has high POD-like activity but easily dissolves into a solution. In their study, the authors first modified the electrode surface with a mixture of Fe₃O₄@ZIF-8 and MoS₂ nanosheets. Then, gold nanoflowers were deposited on the as-prepared electrode. Under the synergistic work of a MoS₂ nanosheet and Au nanoflowers, using this method greatly promoted the stability, conductivity, and POD-like activity of Fe₃O₄@ZIF-8 [70,71]. The prepared sensor can be stored at room temperature for 7 days and can be used to detect H₂O₂ released from cells with a low RSD (2.1%) (Table 2). A steady current can be achieved by the sensor in 5 s. Huang et al. synthesized a nanocomposite with POD-like activity, which was made up of rime-like Cu₂(OH)₃NO₃-wrapped ZnO nanorods [Cu₂(OH)₃NO₃@ZnO] [72]. The nanocomposite was grown in situ on an activated graphene fiber (diameter: 50 μm) to develop a flexible and biocompatible microelectrode for the electrochemical detection of H₂O₂ in human colon cells with an LOD of 1 μM and a sensitivity of $272 \mu\text{A mM}^{-1} \text{cm}^{-2}$. The resulting sensor maintains 90% of

its response after 4 weeks, which shows good stability (Table 2). Moreover, when H_2O_2 is added, 95% of the steady signal can be attained in 3 s. This fast response is very beneficial in practical applications.

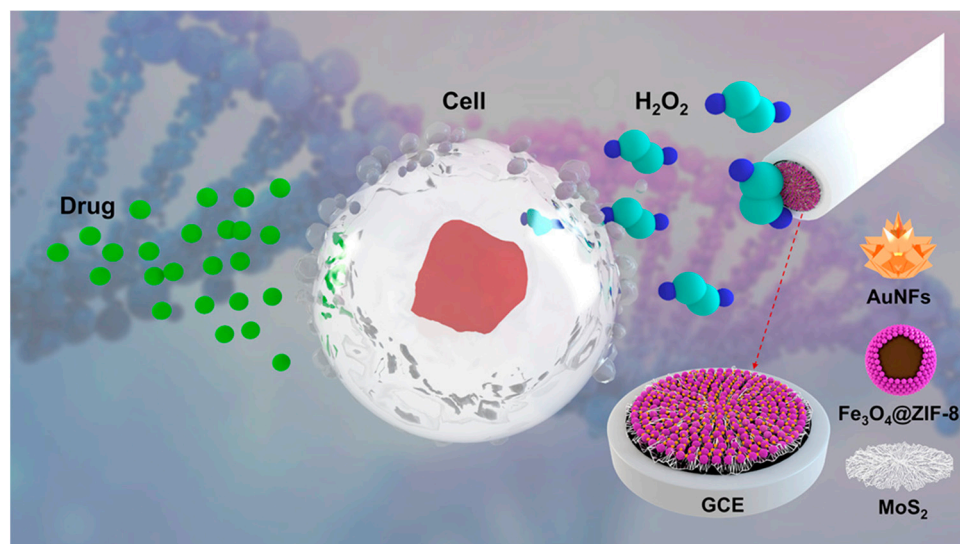


Figure 7. Scheme of an AuNFs/Fe₃O₄@ZIF-8-MoS₂ fabricated H₂O₂ sensor [67]. Copyright: Elsevier B.V.

3.1.2. Sensors for the Oxidation of H₂O₂

Nanomaterials containing one metal element. Pt is the most commonly used metal in H₂O₂ amperometric sensors [73]. Zhu et al. developed a nanozyme by synthesizing platinum nanowires (PtNWs) of about 3 nm in size on peptide nanofibers–biomimetic graphene oxide (PtNWs-PNFs/GO) [74]. After being dispersed in a Nafion solution, they were dried on GCE and an H₂O₂ amperometric sensor was constructed. Good stability was achieved, with a 92% response maintained after storing the sensor at room temperature for 7 days.

Nanomaterials containing bimetallic elements. The scarcity of Pt has motivated scientists to reduce Pt usage in sensor manufacturing. Ceria (CeO₂) is a metal oxide with high redox properties [75]. By reversibly shifting between the Ce⁺³ and Ce⁺⁴ states, CeO₂ has the ability to release or absorb oxygen atoms in different redox environments [76]. Uzunoglu et al. combined the redox properties of CeO₂ (average size: 13.8 nm) with Pt/C inks to develop H₂O₂ amperometric sensors [77]. Pt/C-CeO₂ was first dispersed in Nafion/ethanol/water solution and then dried on the GCE. Pt/C-CeO₂-modified sensors have better electrochemical performance than sensors without CeO₂. When the nanoparticles of CeO₂ and Pt combine, the oxygen storage ability of CeO₂ is reinforced; meanwhile, so is the enzyme-like property of the nanocomposites [78,79]. The best CeO₂ loading content was 20 wt %. The oxidation of H₂O₂ by CeO₂, based on the equation $2\text{CeO}_2 + \text{H}_2\text{O}_2 \rightarrow \text{Ce}_2\text{O}_3 + \text{O}_2 + \text{H}_2\text{O}$, may be another reason for achieving higher activity. The sensor has a sensitivity of $185.4 \mu\text{A mM}^{-1} \text{cm}^{-2}$. After storage at 4 °C for 15 days, the response of the sensor barely changed. The reproducibility of the sensor is also good, with a low RSD = 2.5% (Table 2).

Combining two metal oxides together sometimes also achieves better POD-like properties than single-metal and single-metal-oxide nanoparticles. Using sol-gel methods, Karami et al. first synthesized nickel molybdate (NiMoO₄) with POD-like activity. The NiMoO₄ nanoparticle (average diameter: 32 nm) was dispersed in Nafion solution and then dried on GCE to develop an H₂O₂ sensor [80]. Figure 8 shows the mechanism for the oxidation of H₂O₂ by NiMoO₄. Mo mainly played the role of promoting the electrocatalytic efficiency of NiMoO₄ by improving conductivity, while not being involved in the reaction directly [81–83]. The sensor shows very good stability: after storage for over a month at

room conditions, the response decreased by only about 5%, with acceptable reproducibility (RSD = 3.4%) (Table 2).

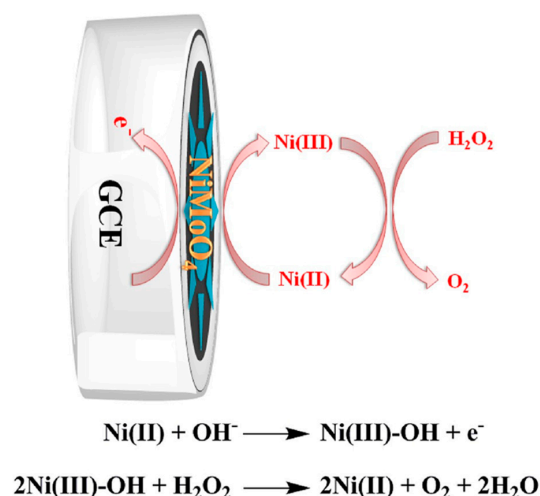


Figure 8. Scheme of NiMnO₄/GCE mechanism to oxidize the H₂O₂ [80]. Copyright: Elsevier B.V.

MOF-based Nanomaterials Portorreal-Bottier et al. prepared a novel 2D MOF material containing metal cobalt (2D-Co-MOF) in a nitrogen coordination environment, dispersing it in Nafion solution before drying it onto the graphite electrode for the electrocatalytic oxidation of H₂O₂ [84]. Due to the coordination effect between cobalt and the nitrogen-metal bonds, 2D-Co-MOF shows good electrocatalysis at a physiological pH. In addition, after the MOF-based material was modified on the electrode, the coordination effect was preserved. This is a unique feature that differs from traditional amperometric H₂O₂ sensors modified with MOFs, which must keep their activity in strongly alkaline conditions. The prepared sensor shows good sensitivity ($501 \pm 3 \mu\text{A mM}^{-1} \text{cm}^{-2}$) (Table 2).

3.1.3. Sensors for the Disproportionation of H₂O₂

Unlike a traditional H₂O₂ sensor based on POD that only reduces H₂O₂, catalase can oxidize H₂O₂ into oxygen while simultaneously reducing it to water [85]. Compared with POD mimics, it is more difficult to construct catalase mimics due to the difficulty of preparing stabilized high-valent metal redox species. Saravanan et al. reported the production of a nanozyme-based H₂O₂ amperometric sensor by the in situ preparation of Mn^{IV/III/II} bipyridyl-aqua complex with catalase-like activity, [Mn^{IV/III/II}(bpy)₂(H₂O)₂]²⁺, on functionalized multiwalled carbon nanotube (CNT)-modified GCE; the mechanism is shown in Figure 9 [86].

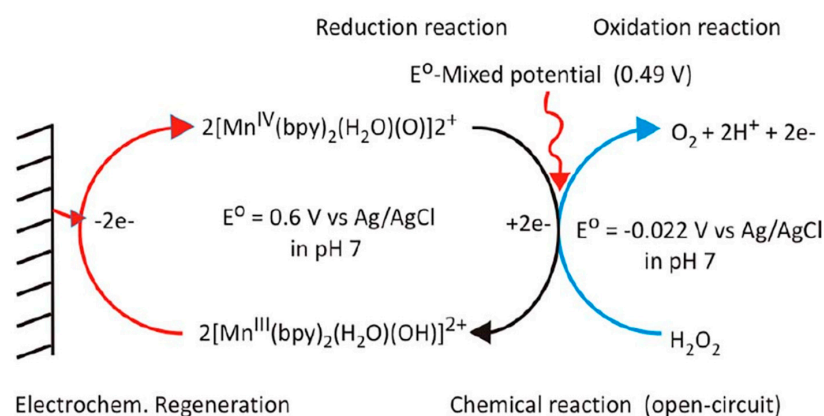


Figure 9. Mechanism of the Mn^{IV/III} mediated electrode process [86]. Copyright: Elsevier B.V.

Table 2. Summary of amperometric sensors using nanozymes for the detection of H₂O₂ (LOD: limit of detection; RSD: relative standard deviation; ^a: data have been normalized by us; /: not reported; Ref.: reference).

Nanozyme	pH	Oxidative or Reductive	Linear Range (mM)	Sensitivity ($\mu\text{A mM}^{-1} \text{cm}^{-2}$)	Potential (V)	RSD %	LOD (μM)	Stability ($^{\circ}\text{C}/\text{Day}$)	Sample	Ref.
Pd@SO ₃ H-MSM	7.4	Reductive	0.047–1000 μM	0.36	−0.04	2.6	0.014	30	Living cells human	[51]
Ag-Mo ₂ C/C	7.4	Reductive	0.08 μM –4.67	466.2	−0.3 v	2.25	0.025	30	serum/disinfectant/contact lens solution	[54]
Ag ₂ MoO ₄ nanowires	7.0	Reductive	0.015–799.2 μM	/	−0.32	<3.5	5.42 nM	4/30	Lens cleaning solution/serum	[55]
Ag/N-Ti ₃ C ₂	7.0	Reductive	0.05–35	552.62	−0.5	3.1	1.53	/	fetal bovine serum	[56]
RGO/nAPAMSs	7.0	Reductive	0.005–4.0	1117.0	−0.5	3.2	0.008	30	Disinfected fetal bovine serum	[57]
SiO ₂ /APTMS/AuPt	7.4	Reductive	5–72,000 μM	46.7	−0.20	8.09	2.6	RT/7	/	[58]
AuPd@Fe _x O _y	7.4	Reductive	50 μM ~1	120.7	−0.2	0.63	3.0	RT/20	Living cells	[59]
AuNPs/Cu-HHTP-NSs	7.4	Reductive	50 nM–16.4	188.1	−0.6	3.1	0.0056	28	Living cells	[62]
Co-NC RDSs	7.4	Reductive	0.001–30	234.913	−0.3	1.78	0.143	60	/	[66]
AuNFs on Fe ₃ O ₄ @ZIF-8-MoS ₂	7.4	Reductive	0.005–120	/	−0.55	2.1	0.9	RT/7	H9C2 cells	[67]
Cu ₂ (OH) ₃ NO ₃ @ZnO	7.4	Reductive	1 μM ~17.4	272	−0.8	5	1	28	Living cells	[72]
PtNWs-PNFs/GO	13	Oxidative	0.1 μM –0.01	/	0.65	/	0.0206	RT/7	/	[74]
Pt/C-CeO ₂	7.4	Oxidative	0.01–30	185.4 \pm 6.5	−0.4	2.5	2	4/15	Disinfectant	[77]
NiMoO ₄	13	Oxidative	0.0001–1.55	/	0.6	3.4	0.01	RT/30	Tap water/river water	[80]
Co-MOF@Nafion	7	Oxidative	0.005–10	^a 501 \pm 3	0.9	3.2/6.1	/	/	Lens cleaning solutions/disinfectant	[84]
GCE/ <i>f</i> -MWCNT@Mn(bpy) ₂ (H ₂ O) ₂	7	Disproportionation	0.02–0.2	^a 0.417	0.65	3.9	1		Clinical sample	[86]

3.2. Sensors Targeting the Detection of Glucose

Nanomaterials containing one metal element. By modifying GCE with a nanocomposite composed of copper and carbon black, Sukhrov et al. successfully manufactured a glucose amperometric sensor without using natural enzymes [87]. The prepared sensor has a good sensitivity of $1595 \mu\text{A mM}^{-1} \text{cm}^{-2}$ and can be stored in room temperature for 30 days for only a 2.4% signal decrease (Table 3). Dilmac et al. deposited AuNPs on a support material of carboxylated graphene oxide (GO-COOH). The obtained GO-COOAu nanocomposite was utilized as GOX mimics in order to construct a glucose sensor in an alkaline medium [88]. The resulting sensor has great potential to be applied in home-based glucose diagnostics, with an acceptable RSD (4.5%); it achieved a steady current in 3 s and can be stored at 4 °C for 30 days (Table 3). Nickel foam is a porous material that is widely used in acoustic absorption and fuel cells. Hayat et al. utilized its porosity to enhance the GOX-like performance of nanozymes, which were then employed to construct amperometric sensors. The developed NiO electrode shows better stability when stored in 0.1 M NaOH than when stored in air (20 days) and shows very good reproducibility, with an RSD = 1.5% (Table 3) [89]. Vivekananth et al. constructed a nanozyme-based amperometric glucose sensor by utilizing a Co_3O_4 /graphene nanocomposite, which combined the advantages of self-assembled graphene stacks and Co_3O_4 NPs (average crystalline size: 15–20 nm) [90]. This Co_3O_4 /graphene-based sensor suffered a current loss of only 5.6% after being stored in an airtight container at room temperature for 60 days, showing very good stability. Besides this, the sensitivity of the sensor is very high and can achieve $2477 \mu\text{A mM}^{-1} \text{cm}^{-2}$ (Table 3). Sridara et al. prepared a nanocomposite with carbon nanodots (2 nm) and CuO [91]. The nanocomposite shows good GOX-like activity after being fabricated on SPCE to detect glucose. No obvious decrease in response after 12 days has been found when storing the sensor at room temperature. The reproducibility of the sensor is also good, and a low RSD = 2.6% was obtained (Table 3). Xie et al. prepared a nanocomposite with a 3D structure using a metallic nickel nitride nanosheet (Ni_3N NS) and Ti mesh [92]. The 3D nanocomposite demonstrated GOX-like activity in alkaline solutions. When synthesizing this 3D nanozyme, Ti was used as a substrate, directly growing the Ni_3N nanosheet onto it. This method guaranteed an intense interaction between Ni_3N and Ti, and the 3D structure enabled electrolytes to diffuse effectively in the composite and more catalytic sites were exposed, which greatly promoted the glucose sensor's performance. The developed sensor had acceptable reproducibility (RSD = 4.7%) and achieved an outstanding sensitivity of $7688 \mu\text{A mM}^{-1} \text{cm}^{-2}$, which is the highest value found in Table 3. The response time of the sensor to achieve a steady signal is less than 5 s. After being stored at room temperature for 30 days, the response only decreased by 8.7%, which was indicative of great stability. Pal et al. prepared a nanozymatic glucose sensor combining $\text{Ni}(\text{OH})_2$ and NiO nanomaterials [93]; the related amperometric parameters of the developed sensor are also listed in Table 3.

Table 3. Summary of amperometric sensors using nanozymes for the detection of glucose (LOD: limit of detection; RSD: relative standard deviation; ^a data have been normalized by us; /: not reported; CV: coefficient of variation).

Nanozyme	Linear Range (mM)	LOD (μM)	Sensitivity ($\mu\text{A mM}^{-1} \text{cm}^{-2}$)	RSD (%)	Stability ($^{\circ}\text{C}/\text{day}$)	Potential(V)	Sample	Ref.
Cu/DCB	0.5–7000 μM	0.1	1595	/	RT/30 D	0.5	serum	[87]
GO-COOAu	0.02–4.58	6	20.218	4.5	4/30 D	0.35	serum	[88]
NiO	0.0554–0.9	1	^a 12.5	1.5	20 D	0.38	/	[89]
Co_3O_4 / graphene	16 μM –1.3	0.5	^a 2477	/	RT/60	0.58	urine	[90]
PDDA/CuO-C-dot	0.5–2, 2–5	0.2 mM	110, 63.3	2.6	RT/12	0.5	serum	[91]
Ni_3N NS/Ti	0.2 μM –1.5 mM	0.06	7688	4.7	RT/30	0.55	serum	[92]
$\text{Ni}(\text{OH})_2$ nano and NiO nanorods	0.1–156, 0.01–83	70 and 8.1	12.09, 24.0	/	/	0.52	serum	[93]
Au/Ni	10 μM –20	5.84	0.96 $\mu\text{A}/\text{mM}$	CV = 2.93%	18 D	0.4	human blood	[94]
HNPG/AuSn	2 μM –8.11	0.36	4374.6	3.9	4/42 D	0.1	serum	[95]
Cu_2O -Au NCMs	5 μM –2.385	0.76	^a 1630	/	/	0.5	orange juice	[96]
ZnO NRs/ Fe_2O_3 /nafion	^a 5.56–22.2 mg/dL	0.95 mM	^a 0.00289	/	/	0.7	/	[97]

Table 3. Cont.

Nanozyme	Linear Range (mM)	LOD (μM)	Sensitivity ($\mu\text{A mM}^{-1} \text{cm}^{-2}$)	RSD (%)	Stability ($^{\circ}\text{C}/\text{day}$)	Potential(V)	Sample	Ref.
Bronze	0–320 μM	6.64	482	10%	RT/5	0.65	saliva	[98]
PANINS@rGO	1–4000 μM	0.03	3448.27	0.96	/	/	/	[99]
RGO-AuNCs@CuO	0.1 μM –3	0.03	/	1.2–2.9	4/60	0.31	serum	[100]
NiCo/C	0.5 μM –4.38	0.2	265.53	2.21–2.69	30 D	0.5	serum	[101]
CC@CCH MOF LDH	0.001–2	0.11	4310	/	/	0.55	/	[102]
NiCo NSs/GNR-GC	5 μM –0.8, 1–10	0.6	344	/	RT/21	0.6	serum	[103]
AuNPs/CuO	0.5 μM –5.67	0.5	872.71	4.71	24 D	0.6	serum	[104]
NWs-MoS ₂								
Cu ₂ O-Cu-Au	0–4.5	1.71	1082	/	7	0.6	serum	[105]

Nanomaterials containing bimetallic elements. As described in the section on H₂O₂ sensors (3.1), combining some single metals or metal oxides together is likely to obtain better catalytical activity. Au/Ni alloy was used by Lee et al. for its GOX-like activity at a neutral pH to develop a glucose sensor (Figure 10) [94]. The reproducibility of the sensor was good since the obtained coefficient of the variation value was 2.93 % ($n = 5$). The upper limit of the linear range of the sensor was 20 mM (Table 3), which covered the human glucose reference value, showing good potential for human blood assay. Nanoporous gold (NPG) has an enhanced GOX-like property due to its large surface area. NPG-modified electrodes can be used to detect glucose directly. Unlike the commonly used pure Au, Pei et al. employed nanoporous Au₈₀Sn₂₀ (wt %) alloy, which has a surface area 7 times larger than traditional NPG based on gold only, to fabricate an electrode, which thus demonstrated better GOX-like activity [95]. The as-prepared sensor needs less than 4 s to achieve a steady current. It has an ultrahigh sensitivity of 4374.6 $\mu\text{A mM}^{-1} \text{cm}^{-2}$, a wide linear range of 2 μM to 8.11 mM, and good reproducibility (RSD = 3.9%). The sensor also has good stability; after being stored at 4 $^{\circ}\text{C}$ for 6 weeks, the response only decreased by 7% (Table 3). Praveen et al. developed a nanocomposite material by directly synthesizing Au NPs on Cu₂O (Cu₂O-Au NCMs); then, the nanocomposite (average size: ~20 nm) was employed in the amperometric detection of glucose [96]. AuNPs themselves show GOX-like activity to a certain extent. Similar to CuO, Cu₂O can also be used to develop GOX-like nanozymes. In this case, Cu₂O acts as a template to grow AuNPs in situ. However, the synergistic effect of Au NPs and Cu₂O endowed the nanocomposite with more outstanding GOX-like activity. Cu₂O-Au NCMs electrodes have a sensitivity of 1630 $\mu\text{A mM}^{-1} \text{cm}^{-2}$ (Table 3). Marie et al. first grew zinc oxide nanorods (NRs) on an FTO substrate. Furthermore, Fe₂O₃ was fabricated on the ZnO NRs to expose more active sites, which facilitated glucose detection [97]. Chen and his coworkers developed an amperometric glucose sensor using the alloy of Sn and Cu [98]. The sensor was integrated into a toothbrush-like form to detect glucose in human saliva and could be stored at room temperature for 5 days. With the help of the sensor, the authors found that the glucose level in saliva correlated well with the blood glucose level.

Reduced graphene oxide (RGO) can also be used as a support material to develop a GOX-like nanozyme. Through the layer-by-layer polymerization of polyaniline nanosheets on RGO (PANINS@RGO), Kailasa et al. successfully developed a glucose sensor without using natural enzymes [99]. The developed glucose sensor had a very low LOD of 0.03 μM , high sensitivity of 3448.27 $\mu\text{A mM}^{-1} \text{cm}^{-2}$, and very good reproducibility, with an RSD of only 0.96%. Liu et al. reported a 3D nanocomposite that still utilized RGO (average size: ~220 nm) as the support while combining it with CuO (diameter: 1–5 nm) and Au nanocrystals (RGO-Au NCs@CuO) [100]. This study integrated the properties of the three single nanomaterials, thus providing a good amperometric glucose sensor based on nanozymes; it has a wide linear range from 0.1 μM to 3 mM, acceptable reproducibility (RSD < 3%), and good stability, in that the response decreased by only 2.72% after being stored at 4 $^{\circ}\text{C}$ for over 2 months (Table 3).

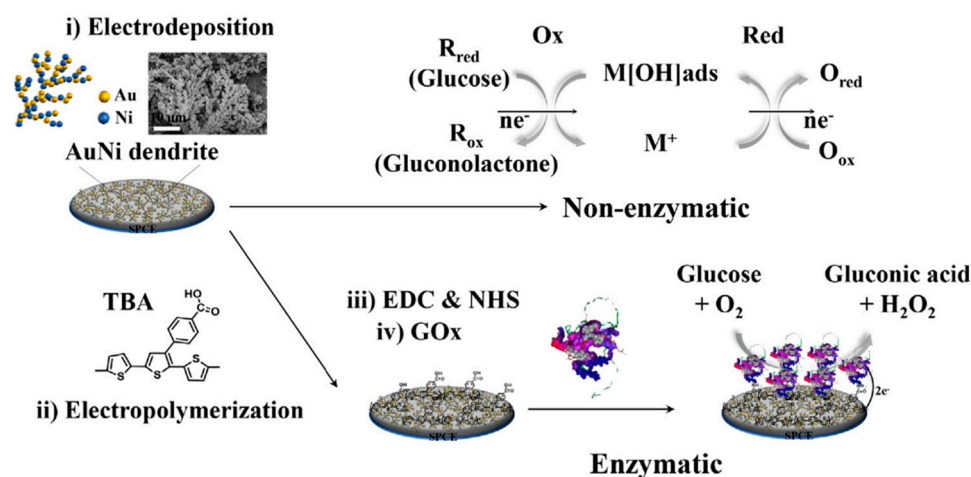


Figure 10. Scheme of the sensor fabrication and mechanism for glucose determination [94]. Copyright: Elsevier B.V.

MOF-based nanomaterials. Wang et al. first synthesized a NiCo MOF, then the resulting MOF material underwent calcination in N_2 to uniformly distribute the carbon in the alloyed Ni/Co NPs (Figure 11) [101]. The prepared composite (NiCo-MOF) was used to fabricate screen-printed carbon electrodes (SPCE). The developed sensor manifested good GOX-like activity and an acceptable RSD ($<3\%$) and could be stored at $4\text{ }^\circ\text{C}$ for 30 days (Table 3). Song et al. designed a nanocomposite CC@CCH MOF LDH with a 3D hierarchical structure to achieve good glucose sensing performance without using natural enzymes [102]. The 3D composites contained cobalt carbonate hydroxide nanorods (CCH), Ni/Co layered double hydroxides (LDH), and carbon cloth (CC). The author first utilized carbon cloth as a substrate to prepare CCH nanorods (average diameter: $\sim 50\text{ nm}$). Next, the CCH acted as a template to grow ZIF-67. Finally, the ZIF-67 was used as a template to synthesize Ni/Co layered double hydroxides. The 3D morphology exposed more catalytical sites, thus achieving better GOX-like activity. The sensitivity of the CC@CCH MOF LDH-based glucose sensor is good, at $4310\text{ }\mu\text{A mM}^{-1}\text{ cm}^{-2}$ (Table 3), and it can achieve a steady response in 6 s. Using ZIF-67 MOF nanocrystals as a template, Asadian et al. synthesized NiCo LDH nanosheets (average size: $\sim 550\text{ nm}$) with a flower-like appearance (Figure 12). Graphene nanoribbons were prepared by unzipping multi-walled CNTs. The obtained nanoribbon worked as a binder to the GCE. Combined with flower-like nanosheets, the fabricated sensor demonstrated good glucose-sensing performance in alkaline solutions, with a sensitivity of $344\text{ }\mu\text{A mM}^{-1}\text{ cm}^{-2}$ [103]. The sensor also has good stability; after being stored at room temperature for 3 weeks, the response only decreased by 7% (Table 3). The response of the sensor is also rapid and a steady current can be achieved in 5 s, which is an acceptable speed for practical use.

Nanomaterials containing multiple metal elements. Copper oxide nanowires not only have good conductivity but also a large surface area, thus giving them their GOX-like activity. MoS_2 has a layered structure; furthermore, it has defects and edges with an abundance of active sulphur, making it easy to combine with AuNPs. Bao and his coworkers developed a nanozymatic glucose sensor, based on nanocomposites, which has a conductive network that combines the advantages of CuO nanowires (diameter: 200 nm , length: $30\text{ }\mu\text{m}$), MoS_2 , and AuNPs [104]. The AuNPs/CuONWs- MoS_2 -based glucose sensor has a wide linear range from $0.5\text{ }\mu\text{M}$ to 5.67 mM , a good sensitivity of $872.71\text{ }\mu\text{A mM}^{-1}\text{ cm}^{-2}$, acceptable reproducibility (RSD = 4.71%), and great stability (the response decreased by $<4\%$ after 24 days). Pu et al. developed a ternary flower-like $\text{Cu}_2\text{O-Cu-Au}$ (CCAu) and used it as sensor material to detect glucose [105]. Au NPs were loaded onto the surface of flower-like $\text{Cu}_2\text{O-Cu}$ nanomaterials. The sensor had good sensitivity ($1082\text{ }\mu\text{A mM}^{-1}\text{ cm}^{-2}$) and acceptable stability, maintaining a 93% response for 7 consecutive days (Table 3).

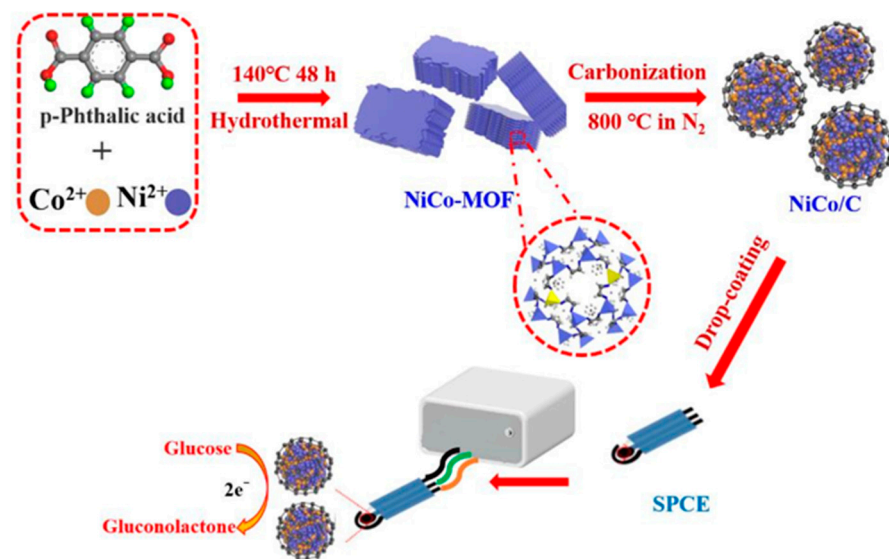


Figure 11. Scheme of the preparation process of the NiCo/C–based assay for glucose determination [101]. Copyright: John Wiley and Sons.

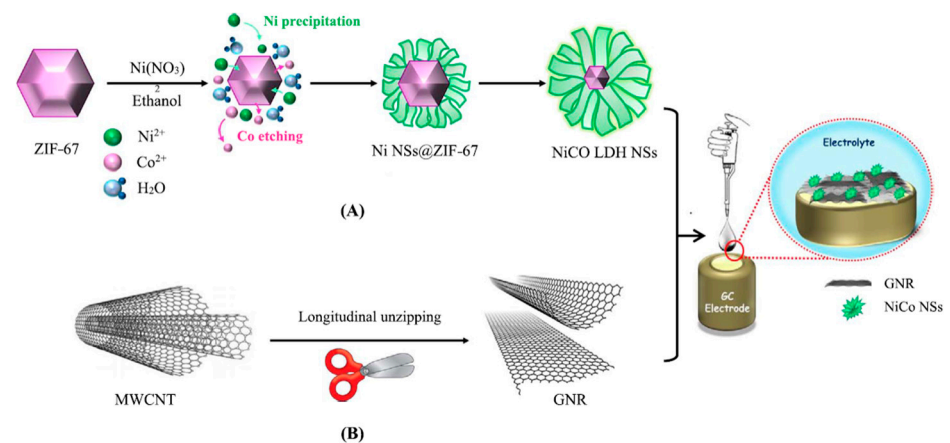


Figure 12. Scheme of the GC electrode modification procedure: (A) the synthesis of NiCo LDH NSs and (B) the preparation of narrow graphene nanoribbons [103]. Copyright: Elsevier B.V.

3.3. Sensors Combining Natural Enzymes with Nanozymes

Thousands of enzymes have been discovered in the human body and it is impossible for scientists to mimic all such natural enzymes within a short period. Considering the fact that peroxidase mimics are the most mature nanozymes that have been developed, and considering their wide application in analytical science, scientists have invented sensors combining the advantages of enzymes drawn from natural resources and the advantages of enzyme-mimics based on nanomaterials. Colozza's group prepared a sulfur mustard sensor combining the properties of choline oxidase enzyme (ChOx, the by-product of which was H_2O_2) and Prussian blue (Figure 13) [106]. The activity of ChOx will be inhibited by the mustard, while Prussian blue promotes the performances of H_2O_2 amperometric sensors, due to its renowned POD-like activity. The prepared sensor should be used within 24 h when stored at room temperature.

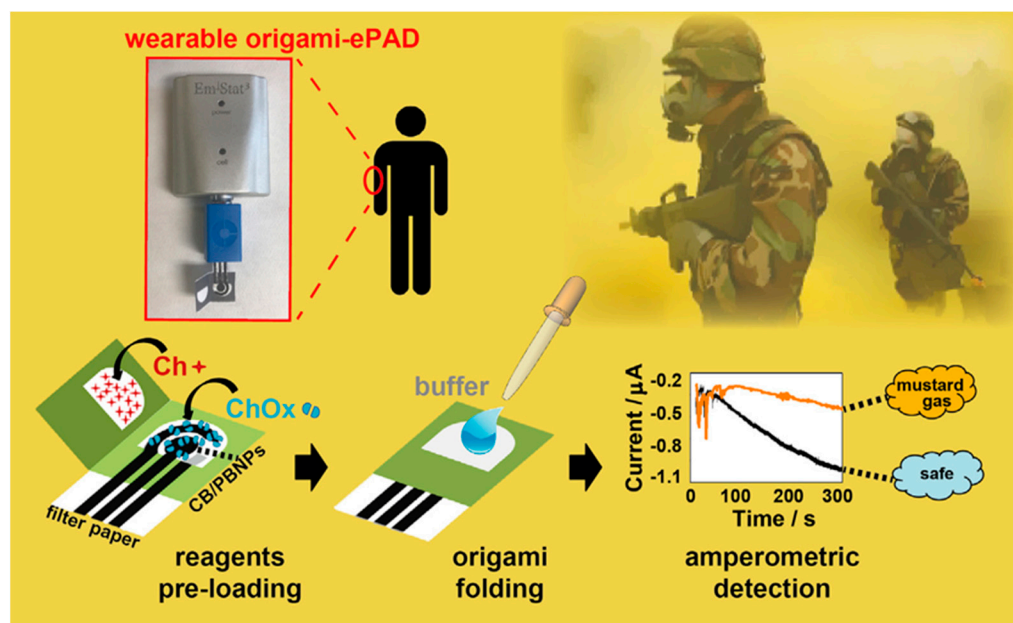


Figure 13. Working principle of the developed wearable mustard gas sensor [106]. Copyright: Elsevier B.V.

Bilgi et al. used alcohol dehydrogenase (ADH) and alcohol oxidase (AOx) as selective enzymes to detect ethanol, methanol, and their mixtures [107]. A biosensor fabricated with ADH can only detect ethanol, while a biosensor fabricated with AOx can detect both methanol and ethanol. Multiwalled carbon nanotubes (MWCNTs), gold nanoparticles, and polynuclear red (PNR) film were modified on SPCE to improve conductivity and act as a mediator. Moscone's group prepared a paper-based amperometric sensor to detect active ingredients in pesticides by taking advantage of the ability of different types of pesticides to inhibit butyrylcholinesterase, alkaline phosphatase, and tyrosinase, respectively [108]. When applied in order to assay 2,4-dichlorophenoxyacetic acid and atrazine, the electrodes were fabricated with carbon black alone. When applied in order to assay paraoxon, the electrode was fabricated with PB NPs. The use of carbon black or PB NPs can help the sensors to achieve better sensitivity and work at a low applied potential.

Elsewhere, 3D pyrolytic carbon microelectrodes coated with RGO have been used as a substrate to develop amperometric sensors. When functionalized with GOX, a glucose sensor can be achieved [109]. A decrease of 8% was observed after storing the prepared sensors in 4 °C for 7 days. SnO₂ is widely used in solar cells for its high electron mobility. In Kafi's work, they mixed GOX and multiparous nanofibers of SnO₂ together. Then, with the help of chitosan, they dried the mixture on gold electrodes modified with PB [110]. GOX worked to produce H₂O₂, which would then be catalyzed on the electrode with PB. A steady signal can be attained after less than 10 s. Moreover, the obtained sensor has very good stability; only a 5% decrease in response was observed after 30 days when it was stored at 4 °C.

Taking advantage of the Cu nanoflowers, a novel nanomaterial was designed by Fang et al. to construct a nanozymatic glucose sensor [111]. Cu nanoflowers can be synthesized by optimizing Cu²⁺ concentration and the deposition duration on the Pt electrode. After successful deposition with the Cu nanoflower, the Pt microelectrode achieved a larger surface area, a lower applied potential to initiate electron transfer, and better POD-like activity to catalyze the H₂O₂ produced by GOX (Figure 14). Consequently, 95% of the steady-state current can be achieved by the sensor within 15 s. The stability of the sensor is also outstanding. When stored at a relatively high temperature of 37 °C, the sensor response increased in the first 6 days but tended to stabilize over the next 14 days.

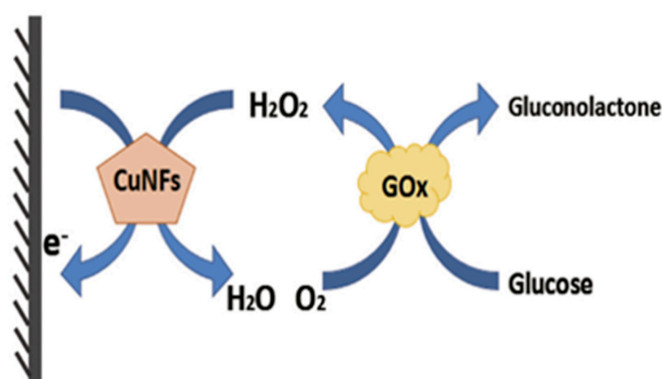


Figure 14. Mechanism of the fabricated Cu nanoflower glucose sensor [111]. Copyright: Elsevier B.V.

Yang's group prepared Pt nanoparticles from PtCl_6^{2-} , using P25, a commercial nano TiO_2 , as a photo reductant [112]. The atomic ratio of Pt in Pt/ TiO_2 is only 1.49%, which greatly reduces the consumption of the novel metal. The Pt NPs distributed on the TiO_2 surface with great dispersion, thus enduing the nanocomposite with outstanding POD-like activity. When H_2O_2 was added, the steady signal could be attained in only 2 s, which is a great advantage when in practical use. With the introduction of lactate oxidase, a lactic acid biosensor was developed. Smutok et al. synthesized a nanozyme with POD-like activity via immobilized hemin and AuNPs on carbon microfibers [113]. Using a coupled nanozyme with natural oxidases, alcohol oxidase (AOX), and glucose oxidase (GOX), the authors developed ethanol sensors and glucose sensors, respectively, which had been successfully used in assays for alcohol and glucose in must and wine.

Xuan et al. electrochemically deposited Au and Pt alloy nanoparticles onto Au electrodes coated with RGO (Au/RGO); naturally derived GOX was immobilized on the electrode with chitosan to develop a wearable sensor that can detect glucose in human sweat (Figure 15) [114]. The authors demonstrated that electrodes fabricated with Au/Pt alloy NPs have a larger surface area and higher POD-like activity. When the sweat sample is added, a steady signal can be attained within 10 s. The developed sensor can still work well after being stored at 4 °C for 8 days. Bollella's group developed a microneedle-based biosensor that can detect lactate continuously [115]. The surface of the needles was fabricated with Au-MWCNTs; then, the methylene blue (MB), which acted as an electron mediator, was successively electropolymerized on the needles. Being immobilized with natural lactate oxidase, such a microneedle can continuously monitor the concentration of lactate in artificial interstitial fluid and human serum. After being stored at 4 °C for 30 days, the response decreased by only 10%, which means that the sensor has great stability.

The summary of the amperometric sensors combining natural enzymes with nanozymes is listed below in Table 4:

Table 4. Summary of the amperometric sensors combining natural enzymes with nanozymes.

Target	Natural Enzyme	Nanozyme	Stability (°C/Day)	Sample	Reference
Sulfur mustard (SM)	ChOx	PBNPs	RT/24 h	SM in aerosol phase	[106]
Ethanol, methanol, and their mixtures	ADH/AOx	MWCNTs/AuNPs/PNR	/	Commercial alcoholic drink	[107]
Organophosphorus insecticides, phenoxy-acid herbicides, and triazine herbicides	butyrylcholinesterase, alkaline phosphatase, and tyrosinase	Carbon black/PB NPs	/	Real-life river water	[108]
Glucose	GOx	Reduced graphene	4/7	Serum	[109]
Glucose	GOx	PB film	4/30	/	[110]
Glucose	GOx	Cu Nanoflower	37/14	Rat skin of cervical dorsal	[111]
Lactate	LOx	Pt/ TiO_2	/	Serum	[112]
Ethanol/Glucose	AOx/GOx	CF-H-Au	/	Grape must/wine	[113]
Glucose	GOx	AuPtNP	4/8	Human sweat	[114]
Lactate	LOx	Au-MWCNTs/polyMB	4/30	Artificial interstitial fluid/human serum	[115]

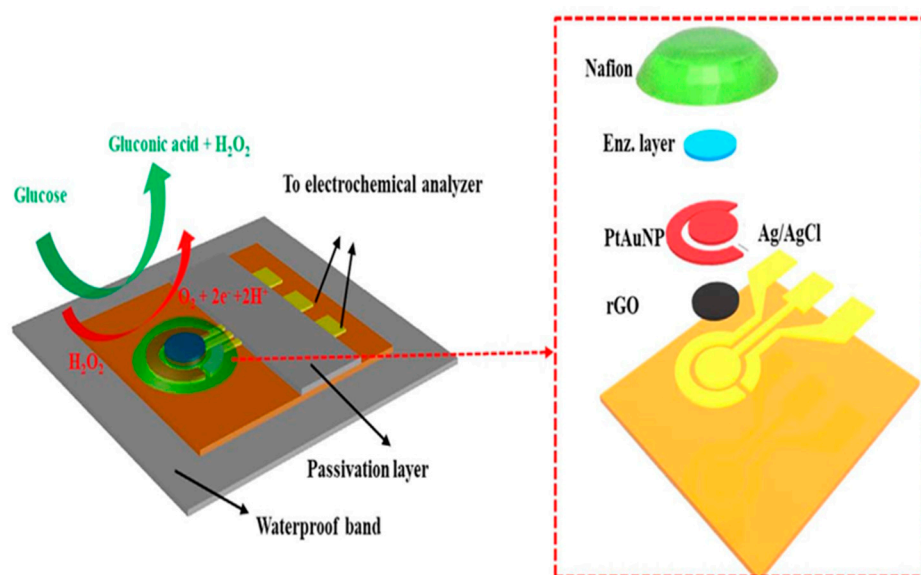


Figure 15. Schematic drawing of the entire human sweat–based wearable glucose sensor, along with an exploded view [114]. Copyright: Elsevier B.V.

3.4. Other Sensors

In addition to presenting specific enzyme-like activities, some nanomaterials can be used to detect bioactive substances by the combined utilization of their nonenzymatic recognition properties with well-designed sensors. The enzyme-like activity changed when such recognition events happened. By utilizing these characteristics, researchers developed enzymatic amperometric sensors to detect specific targets.

Nanomaterials containing one metal element. H_2O_2 can efficiently oxidase 2,2'-azinobis (3-ethylbenzothiazoline-6-sulfonic acid) (ABTS) into green-colored ABTS_{ox} with the help of cobalt oxyhydroxide (CoOOH) nanoflakes possessing POD-like properties. Wen et al. found that through electrostatic absorption and covalent interaction, As(V) can selectively combine with CoOOH nanoflakes [116]; this interaction greatly decreased the POD-like property of CoOOH nanoflakes, reducing the effectiveness with which H_2O_2 oxidized ABTS. Using the specific recognition effect between CoOOH nanoflakes and As(V), an amperometric sensor was prepared to detect As(V) (Figure 16). After storage at 4 °C for 30 days, the sensor response only decreased by 4.2%, demonstrating its good stability. Liu et al. discovered that by surrounding gold nanoclusters with histidine, the prepared nanocomposite had intrinsic oxidase-like properties. Without the presence of H_2O_2 , the nanozyme can oxidize 3,3',5,5'-tetramethylbenzidine (TMB) to ox-TMB directly [117]. The catalytic activity was further enhanced when combining the nanozyme with RGO. However, it is interesting that once the nanozyme contacted nitrite, its strong oxidase-like activity was significantly inhibited when oxidizing TMB. Utilizing this phenomenon, the authors developed an amperometric with which to assay nitrite. The sensor only took under 3 s to achieve 95% of the steady signal. Koo et al. integrated the entire process of circulating tumor nucleic acids (ctNA) target analysis, such as sample processing, nucleic acid amplification, and signal reads, on a single biochip. This work used superparamagnetic Fe_2O_3 particles as stable POD-like nanozymes to oxidase TMB in the presence of H_2O_2 during amperometric measurement [118]. The current intensity is related to the level of the target gene. Using prostate cancer (PC) as a model, the authors demonstrated that simultaneous target analysis of multiple PC genetic aberrations (including gene fusion and overexpression mutations) in human samples can be achieved. Bhattacharjee and his coworkers used mesoporous iron oxide (MIO) with POD-like properties to detect DNA methylation in colorectal cancer cell lines [119]. The author first processed the sample with extracted and denatured target DNA to yield ssDNA, then dropped this onto the gold electrode surface directly. To selectively target the methylcytosine groups, the MIO nanozyme was functionalized with

a 5-methylcytosine antibody (5mC) to act as signal tags. The MIO-5mC nanozyme tag catalyzed the oxidation of TMB by H_2O_2 to achieve the amperometric detection of DNA methylation. The mechanism for the POD-like activity of MIO was supposed to follow the Fenton reaction mechanism. The Fe^{3+} dissociated H_2O_2 into hydroxyl free radicals, which further oxidized the TMB.

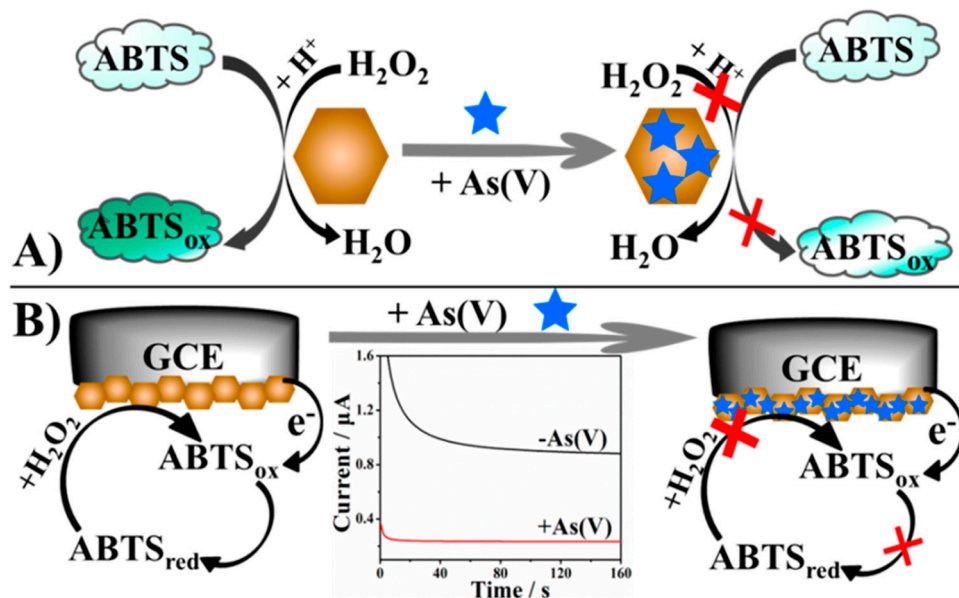


Figure 16. Scheme of arsenate sensors based on CoOOH nanoflakes with POD-like activity: (A) illustration of the colorimetric method; (B) illustration of the electrochemical strategy [116]. Copyright: American Chemical Society.

Wang et al. built a sensing platform using a BC (bacterial cellulose) @DNA- $Mn_3(PO_4)_2$ nanozyme fixed with living cells [120]. The authors found that the nanozyme-based platform had high catalytic properties regarding superoxide anions and excellent biocompatibility for cell adsorption and growth at the same time. Integrating the BC@DNA- $Mn_3(PO_4)_2$ -fabricated SPCE with a well-designed microfluidic channel, the system achieved cell cultivation and the electrical detection of $O_2^{\bullet-}$ in situ from living cells simultaneously.

Nanomaterials containing bimetallic elements. Boriachek and his coworkers synthesized a superparamagnetic material by loading gold onto ferric oxide nanocubes ($Au-NPFe_2O_3NC$). The superparamagnetic nanocomposite has POD-like activity and can be used to direct the isolation and subsequent detection of a specific population of exosomes (Figure 17) [121]. Functionalized with an exosome-related antibody named CD63, the nanocomposite was dispersed with sample liquids, where they worked as “dispersible nanocarriers” to combine the exosomes. After magnetic collection and purification, the nanocomposite-bound exosomes were incubated on SPCE modified with a specific antibody. The POD-like property of the nanocomposite was utilized for the amperometric detection of placenta alkaline phosphatase (PLAP)-specific exosomes in placental cell-conditioned media. In this case, the nanozymes acted as signal tags and provided signal amplification. Liu et al. prepared a nanozyme with POD-like activity using AuPd alloy-modified polydopamine (AuPd-PDA) to electrochemically catalyze the reduction of H_2O_2 . When labeled with an antibody as the recognition element, the nanozyme was utilized to construct an amperometric platform to detect apolipoprotein E4 (APOE4), which is an important risk factor for Alzheimer’s disease (AD) [122]. After storage at 4 °C for 7 days, the response decreased by only 5.1%, demonstrating that the sensor has an acceptable level of stability.

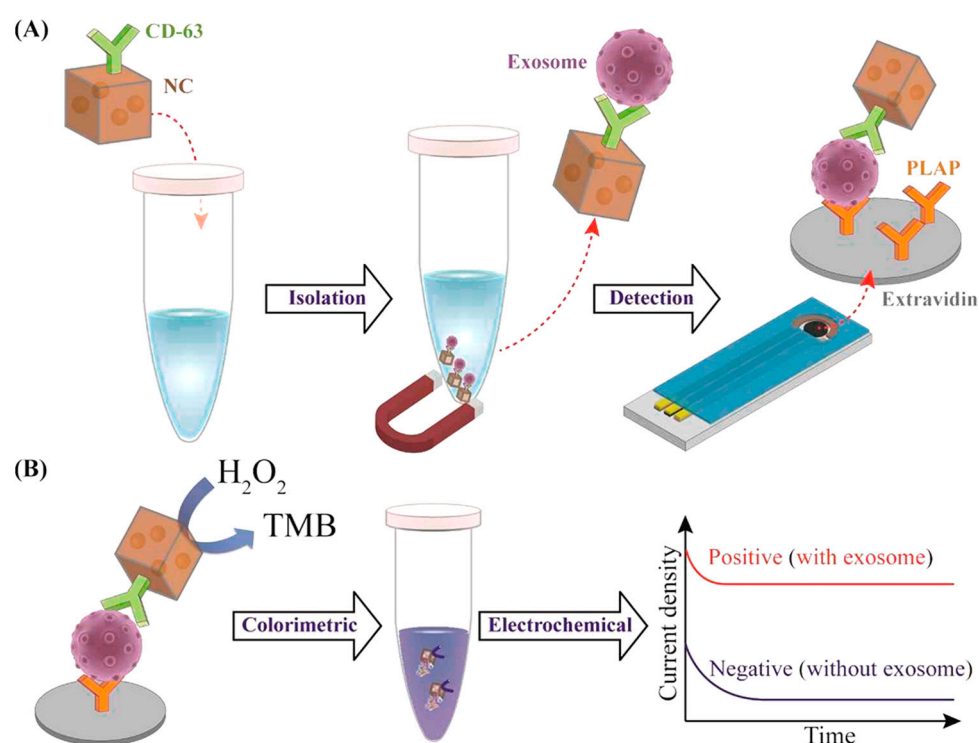


Figure 17. Scheme of the assay for direct exosome isolation and detection from cell culture media [121]. Copyright: American Chemical Society.

Nanomaterials containing multiple metal elements. Li et al. designed a nanocomposite ($MoS_2@Cu_2O-Pt$) by combining MoS_2 nanoflowers, Cu_2O nanocrystals, and Pt NPs. The nanocomposite was used as a nanozyme in developing a hepatitis B surface antigen amperometric sensor (Figure 18) [123]. The synergistic effect presented in $MoS_2@Cu_2O-Pt$ further increased the POD-like activity of the nanozyme to reduce H_2O_2 on the electrode surface, thus improving the detection sensitivity of the immunosensor. After storage at $4\text{ }^\circ\text{C}$ for 30 days, the response decreased by 10%. The acceptable stability may come from the good biocompatibility of the platforms, as described by the author.

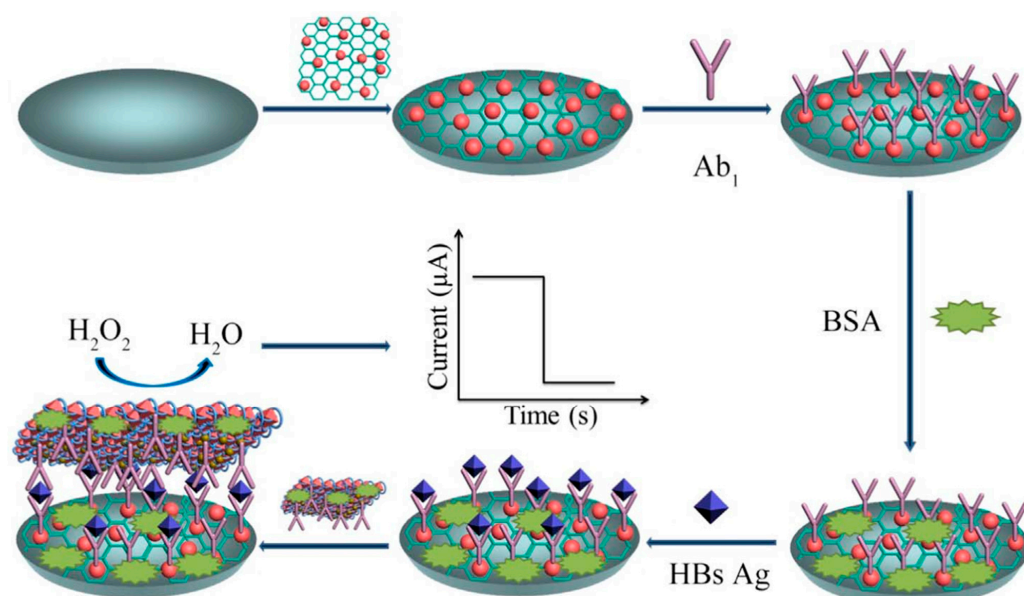


Figure 18. The schematic of the proposed sandwich-type immunosensor, based on $MoS_2@Cu_2O-Pt$ [123]. Copyright: Elsevier B.V.

MOF-based Nanomaterials Lu et al. prepared the Co, N co-doped hierarchical hybrid (Co@NCNTs/NC) nanozyme, which contains both N-doped carbon nanotubes (NCNTs) and N-doped carbon sheets (NC) (Figure 19) [124]. The prepared Co@NCNTs/NC shows comparable oxidase-like activity, which has been applied to construct an amperometric sensor to detect dopamine in human serum and artificial cerebrospinal fluid. The obtained sensor can maintain 90.8% of the current after storage for 30 days at room temperature, which is an outstanding stability result. Xiao et al. modified 2D Cu-TCPP(Fe) with POD-like properties directly onto the electrode surface. However, Cu-TCPP(Fe) is destroyed when in contact with polyethyleneimine (PEI) due to the strong affinity between PEI and Cu^{2+} . This phenomenon greatly decreases the catalytic properties of Cu-TCPP(Fe) [125]. Using this strategy, an amperometric immunosensor based on nanozymes was developed to detect sulfonamides (SAs) in real samples. Liu and his partners prepared “raisin pudding”-type ZIF-67/ $\text{Cu}_{0.76}\text{Co}_{2.24}\text{O}_4$ nanospheres (NSs) by carefully controlling the weight ratio of ZIF-67 and $\text{Cu}(\text{NO}_3)_2$ [126]. In their work, ZIF-67 acted as a template and cobalt source, thus ensuring the successful synthesis of cobalt copper oxide on the surface of ZIF-67/ $\text{Cu}_{0.76}\text{Co}_{2.24}\text{O}_4$ NSs, with multiple enzyme-like activities. The authors developed nanozymatic amperometric sensors to continuously detect 3,4-dihydroxyphenylacetic acid (DOPAC), based on the nanosphere’s laccase-like activity. By assembling Pd NPs on iron-based MOF, Li et al. synthesized a nanozyme and applied it to an amperometric sensor to detect microRNA-122 (a biomarker of liver injury) [127]. The nanohybrids were not only utilized as nanocarriers for the immobilization of signal probes but were also used as redox probes and electrocatalysts. Ren et al. demonstrated that the defects in the MOF structure have a great effect on its catalytic activity. Through a tuning strategy, the defects’ effects on the properties of oxidase-like MOFs were discussed (Figure 20) [128]. Structural defects were introduced into a novel Co-containing zeolitic imidazolate framework with gradually loosened morphology (ZIF-L-Co) by doping cysteine (Cys). With the introduction of more defects, the enzyme-like activities of the materials were effectively promoted. Defects induced by doping with sulfur enhanced the adsorption of O_2 , which further enhanced the oxidase-like properties. ZIF-L-Co-10 mg, with enhanced ascorbate oxidase- and laccase-like properties, was applied to a uric acid (UA) amperometric sensor, which was used to monitor the UA levels in the rat brain continuously. The sensor response was maintained at over 95% after being stored for 30 days, indicating a satisfactory level of stability.

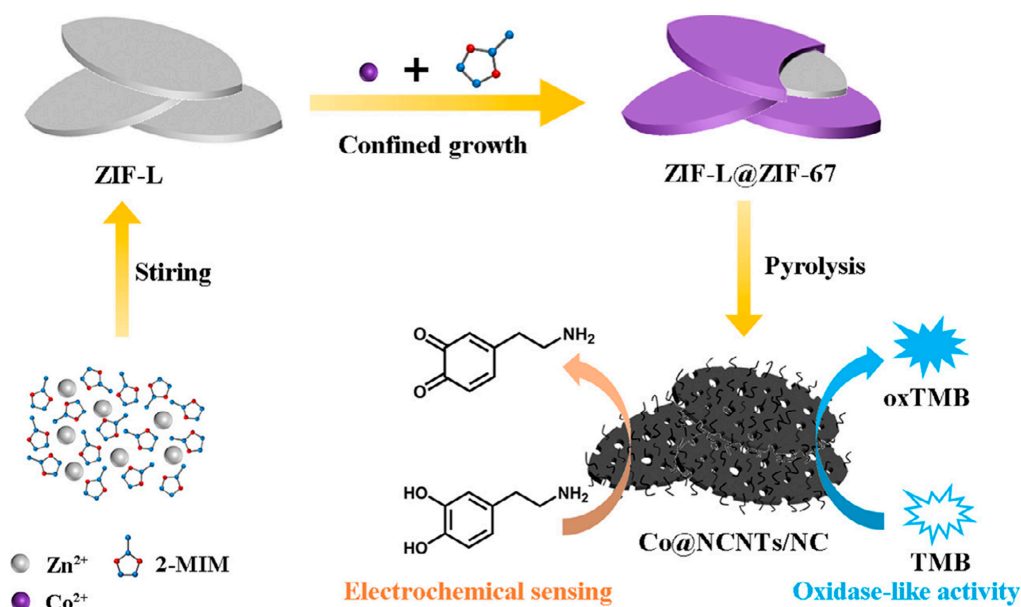


Figure 19. The schematic of the synthesis route of Co@NCNTs/NC and the sensing process [124]. Copyright: Elsevier B.V.

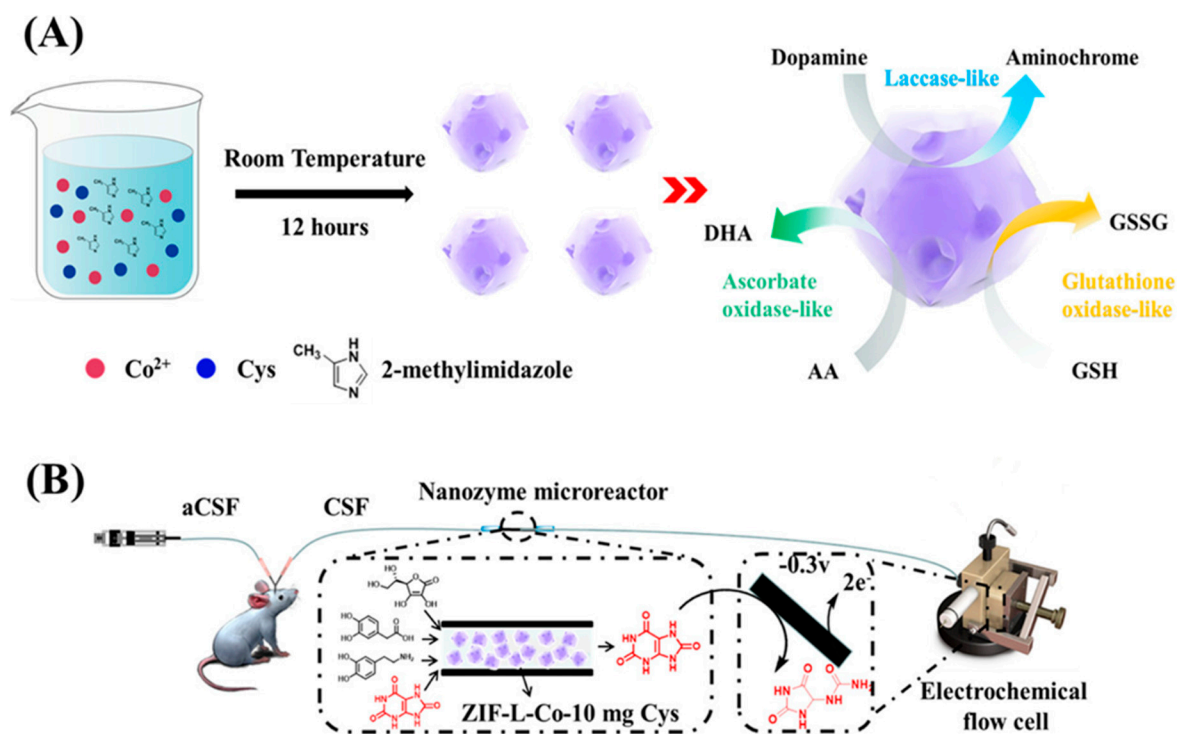


Figure 20. The schematic of (A) the preparation and activities of ZIF-L-Co-10 mg Cys and (B) an online electrochemical analysis of UA [128]. Copyright: American Chemical Society.

The summary of the amperometric sensors detecting untraditional amperometry targets had been listed below in Table 5:

Table 5. Summary of the amperometric sensors detecting untraditional amperometry targets.

Target	Nanozyme	Linear Range	LOD	Stability (°C/day)	Sample Type	Ref.
Arsenate	CoOOH nanoflakes	0.1–200 ppb	56.1 ppt	4/30	Pond slit/paddy soil	[116]
Nitrite	His@AuNCs/RGO	2.5–5700 uM	0.7 uM	/	Sausage	[117]
PC genes	superparamagnetic iron oxide particles	/	50 copies	/	Patient urine and serum	[118]
DNA methylation	MIO	/	10% methylation	/	Colorectal cell line sample	[119]
Superoxide	BC@DNA-Mn ₃ (PO ₄) ₂	34.7 nM–7 uM	5.87 nM	/	A549 cells human nonsmall lung cancer cell line	[120]
Exosomes	Au-NPFe ₂ O ₃ NC	10 ³ –10 ⁷ exosomes/mL	10 ³ exosomes/mL	/	Placental choriocarcinoma cell culture media	[121]
APOE4	AuPd-PDA	0.05–2000 ng mL ⁻¹	15.4 pg mL ⁻¹	4/7	Goat serum	[122]
Hepatitis B surface antigen	MoS ₂ @Cu ₂ O-Pt	0.5 pg/mL–200 ng/mL	0.15 pg/mL	4/28	Serum	[123]
Sopamine	Co@NCNTs/NC	30 nM–710 uM	9 nM	RT/30	Serum/artificial cerebrospinal fluid	[124]
SAs	Cu-TCPP(Fe)	1.186–28.051 ng/mL	0.395 ng/mL	4/15	Real water	[125]
DOPAC	ZIF-67/Cu _{0.76} Co _{2.24} O ₄	0.5–20 uM	0.15 uM	/	Rats' brain microdialysate	[126]
miR-122	PdNPs@Fe-MOFs	0.01 fM–10 pM	0.003 fM	/	Serum	[127]
Uric acid	ZIF-L-Co-10 mg Cys	200 nM–50 uM	67 nM	30	Rat striatum	[128]

4. Challenges and Perspectives

Though great progress has been made, scientists still face several challenges in developing nanozyme-based amperometric sensors. First and foremost, the catalytic activity of current nanozymes is generally lower than that of enzymes from a natural source. Secondly, utilizing the synergetic effect by combining different nanomaterials certainly improves sensor performance. However, considering the lot-to-lot variations found in nanomaterial production, combining several nanomaterials will further enlarge the variations, thus

greatly influencing the reproducibility of sensors between laboratories. Additionally, the processing steps of developing nanocomposite-based amperometric sensors are laborious, which makes it very difficult to apply such sensors in practical applications. Thirdly, the types of nanomaterials are massive and new kinds of nanomaterials are being synthesized almost every day. The traditional way to discover nanocomposites with high catalytic activity by combining nanomaterials is time-consuming and labor-intensive.

Herein, we propose two perspectives for the development of amperometric sensors based on nanozymes. Firstly, interdisciplinary collaboration should be taken seriously in this area; advanced information technology such as machine learning can open a new portal for developing nanozyme-based amperometric sensors. Today, some outstanding works have already employed machine learning in material synthesis and sensor development, but no report has been found by us on developing nanozyme-based amperometric sensors. With the help of machine learning, Zhao et al. realized the simultaneous detection of glucose and insulin in a single sensor. The oxidation potentials of insulin and glucose are very close, meaning that the current signals are mixed and cannot be analyzed using traditional methods. The machine learning algorithms were trained by the extracted features of the cyclic voltammetric curves of glucose and insulin, with known concentrations. Then, the algorithms could be used to calculate the concentrations of glucose and insulin accurately [129]. Giordano et al. used machine learning to overcome the matrix effect. The ethanol sensor that they developed can be applied to a complex sample without the necessity for calibration before use with the help of machine learning [130]. Zhu et al. developed a flexible electrochemical sensor based on nanozymes to detect the ultra-traces of residues of the phytohormone α -naphthalene acetic acid in farmland environments. Using machine learning, the dynamic range of the sensor improved, from 0.02–0.1 μM to 0.02–10 μM [131]. Schroeder et al. developed an electronic nose based on a chemoresistive sensor array fabricated with CNTs. They used machine learning to improve the food classification accuracy of the sensors [132]. Dykstra et al. used machine learning to discover the relationships between synthesis conditions and the corresponding sensing performance. This work first used machine learning to guide the sensing material synthesis [133]. Paul et al. first used machine learning to detect adulteration in metformin hydrochloride [134]. Kalasin and his coworkers developed wearable lab-on-eyeglasses to detect creatinine in tears. Utilizing machine learning, the eyeglasses can distinguish the level of serum creatinine from the tear creatinine with acceptable accuracy [135]. Wang et al. used machine learning to guide the development of new electrode materials for detecting NO_2 . Only five novel materials have been developed in this area in 2018–2020. In their work, with the help of machine learning, the authors selected 400 materials out of 8000 materials. Of these, 13 of the selected materials were used to verify the reliability of the machine learning model. The results proved that the model was reliable [136]. In conclusion, machine learning can be used to improve the performance of developed nanozyme-based amperometric sensors; what is more, it can guide the direction of research and increase the efficiency when developing new nanozymes or nanocomposites, with better activity.

Our second perspective is that the possibility of industrialization and commercialization should be considered when developing nanozyme-based amperometric sensors. New technologies such as the Internet of Things can be used to monitor and automatically control the production process in real time. Besides this, in view of the amperometric sensors detecting glucose, lactic acid, and uric acid based on natural enzymes that are already commercialized, nanozymes should be applied preferentially in such sensors for their relatively mature manufacturing process. When the market has experienced the sweet taste of nanozyme-based amperometric sensors in terms of their lower costs and longer storage periods, more investment will be made to advance research in this area.

5. Conclusions

Amperometry is a subclass of the greater family of electrochemistry; all electrochemical methods referring to potential changes during the detection process have been excluded.

Instead, the most recent advances in nanozyme-based amperometric sensors have been highlighted in this review. Ranged according to the targets of the sensors and the usage of nanozymes, we successively introduced nanozyme-based H₂O₂ sensors, nanozyme-based glucose sensors, sensors combining natural enzymes with nanozymes, and nanozyme-based sensors targeting untraditional specific targets. We also discussed the challenges faced by nanozyme-based amperometric sensors and two perspectives were proposed, which we hope could be helpful in terms of further research in this area.

Author Contributions: Conceptualization, L.T.; writing—original draft preparation, L.T. and L.W.; writing—review and editing, Y.L. and N.G.; investigation—L.T., Y.L. and E.S.; supervision, Y.L. and N.G.; funding acquisition, Y.L. and N.G. All authors have read and agreed to the published version of the manuscript.

Funding: This research was funded by the National Natural Science Foundation of China (51832001 and 61821002), the Natural Science Foundation of Jiangsu Province (BK20222002), and the Nanjing Science and technology development Foundation (202205066).

Institutional Review Board Statement: Not applicable.

Informed Consent Statement: Not applicable.

Data Availability Statement: Not applicable.

Conflicts of Interest: The authors declare no conflict of interest.

References

1. Wang, X.; Dong, S.; Wei, H. Recent advances on nanozyme-based electrochemical biosensors. *Electroanalysis* **2023**, *35*, 38–49.
2. Ronkainen, N.J.; Halsall, H.B.; Heineman, W.R. Electrochemical biosensors. *Chem. Soc. Rev.* **2010**, *39*, 1747–1763.
3. Jia, X.; Dong, S.; Wang, E. Engineering the bioelectrochemical interface using functional nanomaterials and microchip technique toward sensitive and portable electrochemical biosensors. *Biosens. Bioelectron.* **2016**, *76*, 80–90.
4. Xu, Z.; Chen, X.; Dong, S. Electrochemical biosensors based on advanced bioimmobilization matrices. *TrAC Trends Anal. Chem.* **2006**, *25*, 899–908. [[CrossRef](#)]
5. Matthews, C.J.; Andrews, E.S.V.; Patrick, W.M. Enzyme-based amperometric biosensors for malic acid—A review. *Anal. Chim. Acta* **2021**, *1156*, 338218.
6. Sahin, B.; Kaya, T. Electrochemical amperometric biosensor applications of nanostructured metal oxides: A review. *Mater. Res. Express.* **2019**, *6*, 042003. [[CrossRef](#)]
7. Liu, X.; Tong, Y.; Fang, P.P. Recent development in amperometric measurements of vesicular exocytosis. *TrAC Trends Anal. Chem.* **2019**, *113*, 13–24.
8. Hu, J. The evolution of commercialized glucose sensors in China. *Biosens. Bioelectron.* **2009**, *24*, 1083–1089. [[CrossRef](#)]
9. Klatman, E.L.; Jenkins, A.J.; Ahmedani, M.Y.; Ogle, G.D. Blood glucose meters and test strips: Global market and challenges to access in low-resource settings. *Lancet Diabetes Endo.* **2019**, *7*, 150–160.
10. Hassan, M.H.; Vyas, C.; Grieve, B.; Bartolo, P. Recent Advances in Enzymatic and Non-Enzymatic Electrochemical Glucose Sensing. *Sensors* **2021**, *21*, 4672. [[CrossRef](#)] [[PubMed](#)]
11. Nikitina, V.N.; Karastialiova, A.R.; Karyakin, A.A. Glucose test strips with the largest linear range made via single strip modification by glucose oxidase-hexacyanoferrate-chitosan mixture. *Biosens. Bioelectron.* **2023**, *220*, 114851. [[CrossRef](#)]
12. Baranwal, J.; Barse, B.; Gatto, G.; Broncova, G.; Kumar, A. Electrochemical sensors and their applications: A review. *Chemosensors* **2022**, *10*, 363. [[CrossRef](#)]
13. Jacobs, C.B.; Peairs, M.J.; Venton, B.J. Review: Carbon nanotube based electrochemical sensors for biomolecules. *Anal. Chim. Acta* **2010**, *1156*, 338218.
14. Zhang, W.; Ma, D.; Du, J. Prussian blue nanoparticles as peroxidase mimetics for sensitive colorimetric detection of hydrogen peroxide and glucose. *Talanta* **2014**, *120*, 362–367. [[PubMed](#)]
15. Jiang, D.; Ni, D.; Rosenkrans, Z.T.; Huang, P.; Yan, X.; Cai, W. Nanozyme: New horizons for responsive biomedical applications. *Chem. Soc. Rev.* **2019**, *48*, 3683–3704.
16. Wu, J.; Wang, X.; Wang, Q.; Lou, Q.; Li, S.; Zhu, Y.; Qin, L.; Wei, H. Nanomaterials with enzyme-like characteristic (nanozymes): Next-generation artificial enzymes (II). *Chem. Soc. Rev.* **2019**, *48*, 1004–1076. [[PubMed](#)]
17. Huang, Y.; Ren, J.; Qu, X. Nanozymes: Classification, catalytic mechanisms, activity regulation, and applications. *Chem. Rev.* **2019**, *119*, 4357–4412.
18. Gao, L.; Zhuang, J.; Nie, L.; Zhang, J.; Zhang, Y.; Gu, N.; Wang, T.; Feng, J.; Yang, D.; Perrett, S.; et al. Intrinsic peroxidase-like activity of ferromagnetic nanoparticles. *Nat. Nanotechnol.* **2007**, *2*, 577–583. [[CrossRef](#)]
19. Zhang, W.; Hu, S.; Yin, J.J.; He, W.; Lu, W.; Ma, M.; Gu, N.; Zhang, Y. Prussian blue nanoparticles as multienzyme mimetics and reactive oxygen species scavengers. *J. Am. Chem. Soc.* **2016**, *138*, 5860–5865. [[CrossRef](#)]

20. Dong, H.; Du, W.; Dong, J.; Che, R.; Kong, F.; Chen, W.; Ma, M.; Gu, N.; Zhang, Y. Depletable peroxidase-like activity of Fe₃O₄ nanozymes accompanied with separate migration of electrons and iron ions. *Nat. Commun.* **2022**, *13*, 5365.
21. Ai, Y.; Hu, Z.N.; Liang, X.; Sun, H.B.; Xin, H.; Liang, Q. Recent advances in nanozymes: From matters to bioapplications. *Adv. Funct. Mater.* **2022**, *32*, 2110432. [[CrossRef](#)]
22. Zou, W.; Tang, Y.; Zeng, H.; Wang, C.; Wu, Y. Porous Co₃O₄ nanodisks as robust peroxidase mimetics in an ultrasensitive colorimetric sensor for the rapid detection of multiple heavy metal residues in environmental water samples. *J. Hazard. Mater.* **2021**, *417*, 125994. [[CrossRef](#)]
23. Tang, Y.; Hu, Y.; Yang, Y.; Liu, B.; Wu, Y. A facile colorimetric sensor for ultrasensitive and selective detection of Lead (II) in environmental and biological samples based on intrinsic peroxidase-mimic activity of WS₂ nanosheets. *Anal. Chim. Acta* **2020**, *1106*, 115–125. [[CrossRef](#)]
24. Zhang, Z.; Tian, Y.; Huang, P.; Wu, F.Y. Using target-specific aptamers to enhance the peroxidase-like activity of gold nanoclusters for colorimetric detection of tetracycline antibiotics. *Talanta.* **2020**, *208*, 120342. [[CrossRef](#)]
25. Wang, X.; Zhong, X.; Bai, L.; Xu, J.; Gong, F.; Dong, Z.; Yang, Z.; Zeng, Z.; Liu, Z.; Cheng, L. Ultrafine Titanium Monoxide (TiO_{1+x}) Nanorods for Enhanced Sonodynamic Therapy. *J. Am. Chem. Soc.* **2020**, *142*, 6527–6537. [[CrossRef](#)]
26. Boruah, P.K.; Das, M.R. Dual responsive magnetic Fe₃O₄-TiO₂/graphene nanocomposite as an artificial nanozyme for the colorimetric detection and photodegradation of pesticide in an aqueous medium. *J. Hazard. Mater.* **2020**, *385*, 121516. [[CrossRef](#)] [[PubMed](#)]
27. Wang, Y.; Chen, C.; Zhang, D.; Wang, J. Bifunctionalized novel Co-V MMO nanowires: Intrinsic oxidase and peroxidase like catalytic activities for antibacterial application. *Appl. Catal. B Environ.* **2020**, *261*, 118256. [[CrossRef](#)]
28. Cai, S.; Fu, Z.; Xiao, W.; Xiong, Y.; Wang, C.; Yang, R. Zero-Dimensional/Two-Dimensional Au_xPd_{100-x} Nanocomposites with Enhanced Nanozyme Catalysis for Sensitive Glucose Detection. *ACS Appl. Mater. Interfaces* **2020**, *12*, 11616–11624. [[CrossRef](#)]
29. Xi, Z.; Gao, W.; Xia, X. Size Effect in Pd–Ir Core-Shell Nanoparticles as Nanozymes. *ChemElectroChem* **2022**, *21*, 2440–2444. [[CrossRef](#)]
30. Lv, F.; Gong, Y.; Cao, Y.; Deng, Y.; Liang, S.; Tian, X.; Gu, H.; Yin, J.J. A convenient detection system consisting of efficient Au@PtRu nanozymes and alcohol oxidase for highly sensitive alcohol biosensing. *Nanoscale Adv.* **2020**, *2*, 1583–1589. [[CrossRef](#)]
31. Li, S.; Zhao, X.; Gang, R.; Cao, B.; Wang, H. Doping Nitrogen into Q-Graphene by Plasma Treatment toward Peroxidase Mimics with Enhanced Catalysis. *Anal. Chem.* **2020**, *92*, 5152–5157. [[CrossRef](#)] [[PubMed](#)]
32. Xin, Q.; Jia, X.; Nawaz, A.; Xie, W.; Li, L.; Gong, J.R. Mimicking peroxidase active site microenvironment by functionalized graphene quantum dots. *Nano Res.* **2020**, *13*, 1427–1433. [[CrossRef](#)]
33. Zhou, Y.; Zheng, B.; Lang, L.M.; Liu, G.X.; Xia, X.H. Bioinspired Fabrication of Two-Dimensional Metal–Organic Framework-Based Nanozyme for Sensitive Colorimetric Detection of Glutathione. *ACS Appl. Nano Mater.* **2022**, *5*, 18761–18769. [[CrossRef](#)]
34. Huang, L.; Sun, D.W.; Pu, H. Photosensitized Peroxidase Mimicry at the Hierarchical 0D/2D Heterojunction-Like Quasi Metal–Organic Framework Interface for Boosting Biocatalytic Disinfection. *Small* **2022**, *18*, 202200078. [[CrossRef](#)] [[PubMed](#)]
35. Comotti, M.; Pina, C.D.; Matarrese, R.; Rossi, M. The Catalytic activity of “naked” gold particles. *Angew. Chem. Int. Ed.* **2004**, *43*, 5812–5815. [[CrossRef](#)]
36. Chen, Q.; Li, S.; Liu, Y.; Zhang, X.; Tang, Y.; Chai, H.; Huang, Y. Size-controllable Fe-N/C single-atom nanozyme with exceptional oxidase-like activity for sensitive detection of alkaline phosphatase. *Sens. Actuators B Chem.* **2020**, *305*, 127511. [[CrossRef](#)]
37. Li, F.; Li, N.; Xue, C.; Wang, H.; Chang, Q.; Liu, H.; Yang, J.; Hu, S. A Cu₂O-CDs-Cu three component catalyst for boosting oxidase-like activity with hot electrons. *Chem. Eng. J.* **2020**, *382*, 122484. [[CrossRef](#)]
38. Lin, Z.; Zhang, X.; Liu, S.; Zheng, L.; Bu, Y.; Deng, H.; Chen, R.; Peng, H.; Lin, X.; Chen, W. Colorimetric acid phosphatase sensor based on MoO₃ nanozyme. *Anal. Chim. Acta* **2020**, *1105*, 162–168. [[CrossRef](#)]
39. Wang, H.; Yang, W.; Wang, X.; Huang, L.; Zhang, Y.; Yao, S. A CeO₂@MnO₂ core–shell hollow heterojunction as glucose oxidase-like photoenzyme for photoelectrochemical sensing of glucose. *Sens. Actuators B Chem.* **2020**, *304*, 127389. [[CrossRef](#)]
40. Cao, C.; Yang, N.; Su, Y.; Zhang, Z.; Wang, C.; Song, X.; Chen, P.; Wang, W.; Dong, X. Starvation, Ferroptosis, and Prodrug Therapy Synergistically Enabled by a Cytochrome c Oxidase like Nanozyme. *Adv. Mater.* **2022**, *34*, 2203236. [[CrossRef](#)]
41. Zhe, Y.; Wang, J.; Zhao, Z.; Ren, G.; Du, J.; Li, K.; Lin, Y. Ascorbate oxidase-like nanozyme with high specificity for inhibition of cancer cell proliferation and online electrochemical DOPAC monitoring. *Biosens. Bioelectron.* **2023**, *220*, 114893. [[CrossRef](#)] [[PubMed](#)]
42. Dong, W.; Chen, G.; Ding, M.; Cao, H.; Li, G.; Fang, M.; Shi, W. Constructing a novel strategy for one-step colorimetric glucose biosensing based on Co-N_x sites on porous carbon as oxidase mimetics. *Microchem. J.* **2023**, *188*, 108448. [[CrossRef](#)]
43. Ballesteros, C.A.S.; Mercante, L.A.; Alvarenga, A.D.; Facure, M.H.M.; Schneider, R.; Correa, D.S. Recent trends in nanozymes design: From materials and structures to environmental applications. *Mater. Chem. Front.* **2021**, *5*, 7419. [[CrossRef](#)]
44. Ashrafi, A.M.; Bytesnikova, Z.; Berek, J.; Richtera, L.; Adam, V. A critical comparison of natural enzymes and nanozymes in biosensing and bioassays. *Biosens. Bioelectron.* **2021**, *192*, 113494. [[CrossRef](#)]
45. Yang, W.; Yang, X.; Zhu, L.; Chu, H.; Li, X.; Xu, W. Nanozymes: Activity origin, catalytic mechanism, and biological application. *Coordin. Chem. Rev.* **2021**, *448*, 214170. [[CrossRef](#)]
46. Riaz, M.A.; Chen, Y. Electrodes and electrocatalysts for electrochemical hydrogen peroxide sensors: A review of design strategies. *Nanoscale Horiz.* **2022**, *7*, 463. [[CrossRef](#)]

47. Hoffmann, F.; Cornelius, M.; Morell, J.; Fröba, M. Silica-Based Mesoporous Organic–Inorganic Hybrid Materials. *Angew. Chem. Int. Ed.* **2006**, *45*, 3216–3251. [[CrossRef](#)]
48. Pal, M.; Ganesan, V. Zinc Phthalocyanine and Silver/Gold Nanoparticles Incorporated MCM-41 Type Materials as Electrode Modifiers. *Langmuir* **2009**, *25*, 13264–13272. [[CrossRef](#)]
49. Xi, J.; Zhang, Y.; Wang, N.; Wang, L.; Zhang, Z.; Xiao, F.; Wang, S. Ultrafine Pd Nanoparticles Encapsulated in Microporous Co₃O₄ Hollow Nanospheres for In Situ Molecular Detection of Living Cells. *ACS Appl. Mater. Interfaces* **2015**, *7*, 5583–5590. [[CrossRef](#)]
50. Xi, J.; Xie, C.; Zhang, Y.; Wang, L.; Xiao, J.; Duan, X.; Ren, J.; Xiao, F.; Wang, S. Palladium nanoparticles supported on mesoporous silica microspheres for enzyme-free amperometric detection of H₂O₂ released from living cells. *ACS Appl. Mater. Interfaces* **2016**, *8*, 22563–22573. [[CrossRef](#)]
51. Gupta, R.; Singh, P.; Ganesan, V.; Koch, B.; Rastogi, P.K.; Yadav, D.K.; Sonkar, P.K. Palladium nanoparticles supported on mesoporous silica microspheres for enzyme-free amperometric detection of H₂O₂ released from living cells. *Sens. Actuators B Chem.* **2018**, *276*, 517–525. [[CrossRef](#)]
52. Liu, G.; Wang, K.; Wang, L.; Wang, B.; Lin, Z.; Chen, X.; Hua, Y.; Zhu, W.; Li, H.; Xia, J. A Janus cobalt nanoparticles and molybdenum carbide decorated N-doped carbon for high-performance overall water splitting. *J. Colloid Interface. Sci.* **2021**, *583*, 614–625. [[CrossRef](#)] [[PubMed](#)]
53. Li, B.; Liu, L.H.; Song, H.Y.; Deng, Z.P.; Huo, L.H.; Gao, S. Carbon-Doping Mesoporous β-Mo₂C Aggregates for Nanomolar Electrochemical Detection of Hydrogen Peroxide. *ACS Appl. Nano Mater.* **2020**, *3*, 7499–7507. [[CrossRef](#)]
54. Li, B.; Wang, X.T.; Liu, L.H.; Zhang, X.F.; Gao, Y.; Deng, Z.P.; Huo, L.H.; Gao, S. Bimetallic MOFs-derived coral-like Ag-Mo₂C/C interwoven nanorods for amperometric detection of hydrogen peroxide. *Microchim. Acta* **2021**, *188*, 234. [[CrossRef](#)] [[PubMed](#)]
55. Jesila, J.A.A.; Umesh, N.M.; Wang, S.F.; Govindasamy, M.; Allothman, Z.A.; Alshgari, R.A. Simple and Highly Selective Electrochemical Sensor Constructed Using Silver Molybdate Nano-Wire Modified Electrodes for the Determination of Oxidative Stress Biomarker in Blood Serum and Lens Cleaning Solution. *J. Electrochem. Soc.* **2020**, *167*, 147501. [[CrossRef](#)]
56. Zhu, B.; An, D.; Bi, Z.; Liu, W.; Shan, W.; Li, Y.; Nie, G.; Xie, N.; Al-Hartomy, O.A.; Al-Ghamdi, A.; et al. Two-Dimensional Nitrogen-Doped Ti₃C₂ Promoted Catalysis Performance of Silver Nanozyme for Ultrasensitive Detection of Hydrogen Peroxide. *ChemElectroChem* **2022**, *9*, e202200050. [[CrossRef](#)]
57. Bai, Z.; Dong, W.; Ren, Y.; Zhang, C.; Chen, Q. Preparation of nano Au and Pt alloy microspheres decorated with reduced graphene oxide for nonenzymatic hydrogen peroxide sensing. *Langmuir* **2018**, *34*, 2235–2244. [[CrossRef](#)]
58. Liu, W.; Hiekel, K.; Hübner, R.; Sun, H.; Ferancova, A.; Sillanpää, M. Pt and Au bimetallic and monometallic nanostructured amperometric sensors for direct detection of hydrogen peroxide: Influences of bimetallic effect and silica support. *Sens. Actuators B Chem.* **2018**, *255*, 1325–1334. [[CrossRef](#)]
59. Dai, M.; Zhu, Q.; Han, D.; Niu, L.; Wang, Z. An electrochemical sensor based on AuPd@Fe_xO_y nanozymes for a sensitive and in situ quantitative detection of hydrogen peroxide in real samples. *Analyst* **2022**, *147*, 5739–5746. [[CrossRef](#)]
60. Niu, X.; Li, X.; Lyu, Z.; Pan, J.; Ding, S.; Ruan, X.; Zhu, W.; Du, D.; Lin, Y. Metal–organic framework based nanozymes: Promising materials for biochemical analysis. *Chem. Commun.* **2020**, *56*, 11338–11353. [[CrossRef](#)]
61. Li, S.; Liu, X.; Chai, H.; Huang, Y. Recent advances in the construction and analytical applications of metal-organic frameworks-based nanozymes. *TrAc Trends Anal. Chem.* **2018**, *105*, 391–403. [[CrossRef](#)]
62. Huang, W.; Xu, Y.; Wang, Z.; Liao, K.; Zhang, Y.; Sun, Y. Dual nanozyme based on ultrathin 2D conductive MOF nanosheets intergraded with gold nanoparticles for electrochemical biosensing of H₂O₂ in cancer cells. *Talanta* **2022**, *249*, 123612. [[CrossRef](#)]
63. Dhakshinamoorthy, A.; Asiri, A.M.; Garcia, H. 2D Metal–Organic Frameworks as Multifunctional Materials in Heterogeneous Catalysis and Electro/Photocatalysis. *Adv. Mater.* **2019**, *31*, 1900617. [[CrossRef](#)]
64. Gutiérrez-Tarriño, S.; Olloqui-Sariego, J.L.; Calvente, J.J.; Espallargas, G.M.; Rey, F.; Corma, A.; Oña-Burgos, P. Cobalt Metal–Organic Framework Based on Layered Double Nanosheets for Enhanced Electrocatalytic Water Oxidation in Neutral Media. *J. Am. Chem. Soc.* **2020**, *142*, 19198–19208. [[CrossRef](#)]
65. Shang, L.; Yu, H.; Huang, X.; Bian, T.; Shi, R.; Zhao, Y.; Waterhouse, G.I.N.; Wu, L.Z.; Tung, C.H.; Zhang, T. Well-Dispersed ZIF-Derived Co,N-Co-doped Carbon Nanoframes through Mesoporous-Silica-Protected Calcination as Efficient Oxygen Reduction Electrocatalysts. *Adv. Mater.* **2016**, *28*, 1668–1674. [[CrossRef](#)]
66. Wu, Z.; Sun, L.P.; Zhou, Z.; Li, Q.; Huo, L.H.; Zhao, H. Efficient nonenzymatic H₂O₂ biosensor based on ZIF-67 MOF derived Co nanoparticles embedded N-doped mesoporous carbon composites. *Sens. Actuators B Chem.* **2018**, *276*, 142–149. [[CrossRef](#)]
67. Lu, J.; Hu, Y.; Wang, P.; Liu, P.; Chen, Z.; Sun, D. Electrochemical biosensor based on gold nanoflowers-encapsulated magnetic metal-organic framework nanozymes for drug evaluation with in-situ monitoring of H₂O₂ released from H9C2 cardiac cells. *Sens. Actuators B Chem.* **2020**, *311*, 127909. [[CrossRef](#)]
68. Sun, D.; Luo, Z.; Lu, J.; Zhang, S.; Che, T.; Chen, Z.; Zhang, L. Electrochemical dual-aptamer-based biosensor for nonenzymatic detection of cardiac troponin I by nanohybrid electrocatalysts labeling combined with DNA nanotetrahedron structure. *Biosens. Bioelectron.* **2019**, *134*, 49–56. [[CrossRef](#)]
69. Luo, Z.; Sun, D.; Tong, Y.; Zhong, Y.; Chen, Z. DNA nanotetrahedron linked dual-aptamer based voltametric aptasensor for cardiac troponin I using a magnetic metal-organic framework as a label. *Microchim. Acta* **2019**, *186*, 374. [[CrossRef](#)] [[PubMed](#)]
70. Du, H.; Zhang, X.; Liu, Z.; Qu, F. A supersensitive biosensor based on MoS₂ nanosheet arrays for the real-time detection of H₂O₂ secreted from living cells. *Chem. Commun.* **2019**, *55*, 9653–9656. [[CrossRef](#)]

71. Manibalan, K.; Han, S.; Zheng, Y.; Li, H.; Lin, J.M. Latent Redox Reporter of 4-Methoxyphenol as Electrochemical Signal Proxy for Real-Time Profiling of Endogenous H₂O₂ in Living Cells. *ACS Sens.* **2019**, *4*, 2450–2457. [[CrossRef](#)]
72. Huang, W.; Xu, Y.; Sun, Y. Functionalized Graphene Fiber Modified With MOF-Derived Rime-Like Hierarchical Nanozyme for Electrochemical Biosensing of H₂O₂ in Cancer Cells. *Front. Chem.* **2022**, *10*, 873187. [[CrossRef](#)] [[PubMed](#)]
73. Debe, M.K. Electrocatalyst approaches and challenges for automotive fuel cells. *Nature* **2012**, *486*, 43–51. [[CrossRef](#)]
74. Zhu, D.; He, P.; Kong, H.; Yang, G.; Luan, X.; Wei, G. Biomimetic graphene-supported ultrafine platinum nanowires for colorimetric and electrochemical detection of hydrogen peroxide. *J. Mater. Chem. B* **2022**, *10*, 9216. [[CrossRef](#)] [[PubMed](#)]
75. Beie, H.J.; GnÖrich, A. Oxygen gas sensors based on CeO₂ thick and thin films. *Sens. Actuators B Chem.* **1991**, *4*, 393–399. [[CrossRef](#)]
76. Uzunoglu, A.; Kose, D.A.; Stanciu, L.A. Synthesis of CeO₂-based core/shell nanoparticles with high oxygen storage capacity. *Int. Nano Lett.* **2017**, *7*, 187–193. [[CrossRef](#)]
77. Uzunoglu, A.; Ipekci, H.H. The use of CeO₂ -modified Pt/C catalyst inks for the construction of high-performance enzyme-free H₂O₂ sensors. *J. Electroanal. Chem.* **2019**, *848*, 113302. [[CrossRef](#)]
78. Gorte, R.J.; Shao, Z. Studies of the water-gas-shift reaction with ceria-supported precious metals. *Catal. Today* **2005**, *104*, 18–24. [[CrossRef](#)]
79. Uzunoglu, A.; Stanciu, L.A. Novel CeO₂-CuO-decorated enzymatic lactate biosensors operating in low oxygen environments. *Anal. Chim. Acta* **2016**, *909*, 121–128. [[CrossRef](#)]
80. Karami, C.; Taher, M.A. A novel enzyme-less amperometric sensor for hydrogen peroxide based on nickel molybdate nanoparticles. *J. Electroanal. Chem.* **2019**, *847*, 113219. [[CrossRef](#)]
81. Unnikrishnan, B.; Umasankar, Y.; Chen, S.M.; Ti, C.C. Indirect determination of water and hydrogen peroxide oxidation by oxygen evolution studies using multiwalled carbon nanotube-nickel oxide film as electrocatalyst. *Int. J. Electrochem. Sci.* **2012**, *7*, 3047–3058.
82. Zhao, C.; Shao, C.; Li, M.; Jiao, K. Flow-injection analysis of glucose without enzyme based on electrocatalytic oxidation of glucose at a nickel electrode. *Talanta* **2007**, *71*, 1769–1773. [[CrossRef](#)] [[PubMed](#)]
83. Mai, L.Q.; Yang, F.; Zhao, Y.L.; Xu, X.; Xu, L.; Luo, Y.Z. Hierarchical MnMoO₄/CoMoO₄ heterostructured nanowires with enhanced supercapacitor performance. *Nat. Commun.* **2011**, *2*, 381. [[CrossRef](#)] [[PubMed](#)]
84. Portorreal-Bottier, A.; Gutiérrez-Tarriñó, S.G.; Calvente, J.J.; Andreu, R.; Roldán, E.; Oña-Burgos, P.; Olloqui-Sariego, J.L. Enzyme-like activity of cobalt-MOF nanosheets for hydrogen peroxide electrochemical sensing. *Sens. Actuators B Chem.* **2022**, *368*, 132129. [[CrossRef](#)]
85. Vainshtein, B.K.; Melik-Adamyan, W.R.; Barynin, V.V.; Vagin, A.A.; Grebenko, A.I. Three-dimensional structure of the enzyme catalase. *Nature* **1981**, *293*, 411–412. [[CrossRef](#)]
86. Saravanan, N.; Mayuri, P.; Huang, S.T.; Kumar, A.S. In-situ electrochemical immobilization of [Mn(bpy)₂(H₂O)₂]²⁺ complex on MWCNT modified electrode and its electrocatalytic H₂O₂ oxidation and reduction reactions: A Mn-Pseudocatalase enzyme bio-mimicking electron-transfer functional model. *J. Electroanal. Chem.* **2018**, *812*, 10–21. [[CrossRef](#)]
87. Sukhrobov, P.; Numonov, S.; Liu, J.; Luo, J.; Mamat, X.; Li, Y.; Wågberg, T.; Hu, G. Rapid Microwave-Assisted Synthesis of Copper Decorated Carbon Black Nanocomposite for Non-Enzyme Glucose Sensing in Human blood. *J. Electrochem. Soc.* **2019**, *166*, B1238–B1244. [[CrossRef](#)]
88. Dilmac, Y.; Guler, M. Fabrication of non-enzymatic glucose sensor dependent upon Au nanoparticles deposited on carboxylated graphene oxide. *J. Electroanal. Chem.* **2020**, *864*, 114091. [[CrossRef](#)]
89. Hayat, A.; Mane, S.K.B.; Shaishta, N.; Khan, J.; Hayat, A.; Keyum, G.; Uddin, I.; Raziq, F.; Khan, M.; Manjunatha, G. Nickel Oxide Nano-Particles on 3D Nickel Foam Substrate as a Non-Enzymatic Glucose Sensor. *J. Electrochem. Soc.* **2019**, *166*, B1602–B1611. [[CrossRef](#)]
90. Vivekananth, R.; Babu, R.S.; Prasanna, K.; Lee, C.W.; Kalaivani, R.A. Non-enzymatic glucose sensing platform using self assembled cobalt oxide/graphene nanocomposites immobilized graphite modified electrode. *J. Mater. Sci. Mater. Electron.* **2018**, *29*, 6763–6770. [[CrossRef](#)]
91. Sridara, T.; Upan, J.; Saianand, G.; Tuantranont, A.; Karuwan, C.; Jakmunee, J. Non-Enzymatic Amperometric Glucose Sensor Based on Carbon Nanodots and Copper Oxide Nanocomposites Electrode. *Sensors* **2020**, *20*, 808. [[CrossRef](#)] [[PubMed](#)]
92. Xie, F.; Liu, T.; Xie, L.; Sun, X.; Luo, Y. Metallic nickel nitride nanosheet: An efficient catalyst electrode for sensitive and selective non-enzymatic glucose sensing. *Sens. Actuators B Chem.* **2018**, *255*, 2794–2799. [[CrossRef](#)]
93. Pal, N.; Banerjee, S.; Bhaumik, A. A facile route for the syntheses of Ni(OH)₂ and NiO nanostructures as potential candidates for non-enzymatic glucose sensor. *J. Colloid Interface Sci.* **2018**, *516*, 121–127. [[CrossRef](#)] [[PubMed](#)]
94. Lee, W.C.; Kim, K.B.; Gurudatt, N.G.; Hussain, K.K.; Choi, C.S.; Park, D.S.; Shim, Y.B. Comparison of enzymatic and non-enzymatic glucose sensors based on hierarchical Au-Ni alloy with conductive polymer. *Biosens. Bioelectron.* **2019**, *130*, 48–54. [[CrossRef](#)]
95. Pei, Y.; Hu, M.; Tu, F.; Tang, X.; Huang, W.; Chen, S.; Li, Z.; Xia, Y. Ultra-rapid fabrication of highly surface-roughened nanoporous gold film from AuSn alloy with improved performance for nonenzymatic glucose sensing. *Biosens. Bioelectron.* **2018**, *117*, 758–765. [[CrossRef](#)] [[PubMed](#)]
96. Praveen, R.; Ramaraj, R. Facile synthesis of hetero-nanostructured cuprous oxide-gold composite material for sensitive enzymeless glucose detection. *J. Electroanal. Chem.* **2019**, *851*, 13454. [[CrossRef](#)]

97. Marie, M.; Manoharan, A.; Kuchuk, A.; Ang, S.; Manasreh, M.O. Vertically grown zinc oxide nanorods functionalized with ferric oxide for *in vivo* and non-enzymatic glucose detection. *Nanotechnology* **2018**, *29*, 115501. [CrossRef] [PubMed]
98. Chen, J.; Zhu, X.; Ju, Y.; Ma, B.; Zhao, C.; Liu, H. Electrocatalytic oxidation of glucose on bronze for monitoring of saliva glucose using a smart toothbrush. *Sens. Actuators B Chem.* **2019**, *285*, 56–61. [CrossRef]
99. Kailasa, S.; Reddy, R.K.K.; Reddy, M.S.B.; Rani, B.G.; Maseed, H.; Sathyavathi, R.; Rao, K.V. High sensitive polyaniline nanosheets (PANINS) @rGO as non-enzymatic glucose sensor. *J. Mater. Sci. Mater. Electron.* **2020**, *31*, 2926–2937. [CrossRef]
100. Liu, Q.; Jiang, Z.; Tang, Y.; Yang, X.; Wei, M.; Zhang, M. A facile synthesis of a 3D high-index Au NCs@CuO supported on reduced graphene oxide for glucose sensing. *Sens. Actuators B Chem.* **2018**, *255*, 454–462. [CrossRef]
101. Wang, L.; Hou, C.; Yu, H.; Zhang, Q.; Li, Y.; Wang, H. Metal Organic Framework-Derived Nickel/Cobalt-Based Nanohybrids for Sensing Non-Enzymatic Glucose. *ChemElectroChem.* **2020**, *7*, 4446–4452. [CrossRef]
102. Song, D.; Wang, L.; Qu, Y.; Wang, B.; Li, Y.; Miao, X.; Yang, Y.; Duan, C. A High-Performance Three-Dimensional Hierarchical Structure MOF-Derived NiCo LDH Nanosheets for Non-Enzymatic Glucose Detection. *J. Electrochem. Soc.* **2019**, *166*, B1681–B1688. [CrossRef]
103. Asadian, E.; Shahrokhan, S.; Zad, A.I. Highly sensitive nonenzymatic glucose sensing platform based on MOF- derived NiCo LDH nanosheets/graphene nanoribbons composite. *J. Electroanal. Chem.* **2018**, *808*, 114–123. [CrossRef]
104. Bao, J.; Qi, Y.; Huo, D.; Hou, J.; Geng, X.; Samalo, M.; Liu, Z.; Luo, H.; Yang, M.; Hou, C. A Sensitive and Selective Non-Enzymatic Glucose Sensor based on AuNPs/CuO NWs-MoS₂ Modified Electrode. *J. Electrochem. Soc.* **2019**, *166*, B1179–B1185. [CrossRef]
105. Pu, F.; Miao, H.; Lu, W.; Zhang, X.; Yang, Z.; Kong, C. High-performance non-enzymatic glucose sensor based on flower-like Cu₂O-Cu-Au ternary nanocomposites. *Appl. Surf. Sci.* **2022**, *581*, 152389. [CrossRef]
106. Colozza, N.; Kehe, K.; Dionisi, G.; Popp, T.; Tsoutsoulopoulos, A.; Steinritz, D.; Moscone, D.; Arduini, F. A wearable origami-like paper-based electrochemical biosensor for sulfur mustard detection. *Biosens. Bioelectron.* **2019**, *129*, 15–23. [CrossRef]
107. Bilgi, M.; Ayranci, E. Development of amperometric biosensors using screen-printed carbon electrodes modified with conducting polymer and nanomaterials for the analysis of ethanol, methanol and their mixtures. *J. Electroanal. Chem.* **2018**, *823*, 588–592. [CrossRef]
108. Arduini, F.; Cinti, S.; Caratelli, V.; Amendola, L.; Palleschi, G.; Moscone, D. Origami multiple paper-based electrochemical biosensors for pesticide detection. *Biosens. Bioelectron.* **2019**, *126*, 346–354. [CrossRef]
109. Hemanth, S.; Halder, A.; Caviglia, C.; Chi, Q.; Keller, S.S. 3D Carbon Microelectrodes with Bio-Functionalized Graphene for Electrochemical Biosens. *Biosensors* **2018**, *8*, 70. [CrossRef]
110. Kafi, A.K.M.; Alim, S.; Jose, R.; Yusoff, M.M. Fabrication of a glucose oxidase/multiporous tin-oxide nanofiber film on Prussian blue-modified gold electrode for biosensing. *J. Electrochem. Soc.* **2019**, *852*, 113550. [CrossRef]
111. Fang, Y.; Wang, S.; Liu, Y.; Xu, Z.; Zhang, K.; Guo, Y. Development of Cu nanoflowers modified the flexible needle-type microelectrode and its application in continuous monitoring glucose in vivo. *Biosens. Bioelectron.* **2018**, *110*, 44–51. [CrossRef]
112. Yang, Q.; Yang, C.; Wang, Q.; Yang, F.; Song, C.; Yang, H. Electrochemical Biosensor Based on Nano TiO₂ Loaded with Highly Dispersed Photoreduced Nano Platinum. *J. Electrochem. Soc.* **2018**, *165*, 2018. [CrossRef]
113. Smutok, O.; Kavetsky, T.; Prokopiv, T.; Serkiz, R.; Wojnarowska-Nowak, R.; Šauša, O.; Novák, I.; Berek, D.; Melman, A.; Gonchar, M. New micro/nanocomposite with peroxidase-like activity in construction of oxidases-based amperometric biosensors for ethanol and glucose analysis. *Anal. Chim. Acta* **2021**, *1143*, 201–209. [CrossRef] [PubMed]
114. Xuan, X.; Yoon, H.S.; Park, J.Y. A wearable electrochemical glucose sensor based on simple and low-cost fabrication supported micro-patterned reduced graphene oxide nanocomposite electrode on flexible substrate. *Biosens. Bioelectron.* **2018**, *109*, 75–82. [CrossRef] [PubMed]
115. Bollella, P.; Sharma, S.; Cass, A.E.G.; Antiochia, R. Microneedle-based biosensor for minimally-invasive lactate detection. *Biosens. Bioelectron.* **2019**, *123*, 152–159. [CrossRef]
116. Wen, S.H.; Zhong, X.L.; Wu, Y.D.; Liang, R.P.; Zhang, L.; Qiu, J.D. Colorimetric Assay Conversion to Highly Sensitive Electrochemical Assay for Bimodal Detection of Arsenate Based on Cobalt Oxyhydroxide Nanozyme via Arsenate Absorption. *Anal. Chem.* **2019**, *91*, 6487–6497. [CrossRef]
117. Liu, L.; Du, J.; Liu, W.E.; Guo, Y.; Wu, G.; Qi, W.; Lu, X. Enhanced His@AuNCs oxidase-like activity by reduced graphene oxide and its application for colorimetric and electrochemical detection of nitrite. *Anal. Bioanal. Chem.* **2019**, *411*, 2189–2200. [CrossRef]
118. Koo, K.M.; Dey, S.; Trau, M. A Sample-to-Targeted Gene Analysis Biochip for Nanofluidic Manipulation of Solid-Phase Circulating Tumor Nucleic Acid Amplification in Liquid Biopsies. *ACS Sens.* **2018**, *3*, 2597–2603. [CrossRef]
119. Bhattacharjee, R.; Tanaka, S.; Moriam, S.; Masud, M.K.; Lin, J.; Alshehri, S.M.; Ahamad, T.; Salunkhe, R.R.; Nguyen, N.T.; Yamauchi, Y.; et al. Porous nanozymes: The peroxidase-mimetic activity of mesoporous iron oxide for the colorimetric and electrochemical detection of global DNA methylation. *J. Mater. Chem. B* **2018**, *6*, 4783. [CrossRef]
120. Wang, Y.; Wang, D.; Sun, L.H.; Zhang, L.C.; Lu, Z.S.; Xue, P.; Wang, F.; Xia, Q.Y.; Bao, S.J. BC@DNA-Mn₃(PO₄)₂ Nanozyme for Real-Time Detection of Superoxide from Living Cells. *Anal. Chem.* **2020**, *92*, 15927–15935. [CrossRef]
121. Boriachek, K.; Masud, M.F.; Palma, C.; Phan, H.P.; Yamuchi, Y.; Hossain, M.S.; Nguyen, N.T.; Salomon, C.; Shiddiky, M.J.A. Avoiding Pre-Isolation Step in Exosome Analysis: Direct Isolation and Sensitive Detection of Exosomes Using Gold-Loaded Nanoporous Ferric Oxide Nanozymes. *Anal. Chem.* **2019**, *91*, 3827–3834. [CrossRef] [PubMed]
122. Liu, Y.; He, G.; Liu, H.; Yin, H.; Gao, F.; Chen, J.; Zhang, S.; Yang, B. Electrochemical immunosensor based on AuBP@Pt nanostructure and AuPd-PDA nanozyme for ultrasensitive detection of APOE4. *RSC Adv.* **2020**, *10*, 7912. [CrossRef] [PubMed]

123. Li, F.; Li, Y.; Feng, J.; Gao, Z.; Lv, H.; Ren, X.; Wei, Q. Facile synthesis of MoS₂@Cu₂O-Pt nanohybrid as enzyme-mimetic label for the detection of the Hepatitis B surface antigen. *Biosens. Bioelectron.* **2018**, *100*, 512–518. [[CrossRef](#)] [[PubMed](#)]
124. Lu, N.; Yan, X.; Gu, Y.; Zhang, T.; Liu, Y.; Song, Y.; Xu, Z.; Xing, Y.; Li, X.; Zhang, Z.; et al. Cobalt-decorated 3D hybrid nanozyme: A catalytic amplification platform with intrinsic oxidase-like activity. *Electrochim. Acta* **2021**, *395*, 139197. [[CrossRef](#)]
125. Xiao, J.; Hu, X.; Wang, K.; Zou, Y.; Gyimah, E.; Yakubu, S.; Zhang, Z. A novel signal amplification strategy based on the competitive reaction between 2D Cu-TCPP(Fe) and polyethyleneimine (PEI) in the application of an enzyme-free and ultrasensitive electrochemical immunosensor for sulfonamide detection. *Biosens. Bioelectron.* **2020**, *150*, 111883. [[CrossRef](#)] [[PubMed](#)]
126. Liu, J.; Zhang, W.; Peng, M.; Ren, G.; Guan, L.; Li, K.; Lin, Y. ZIF-67 as a Template Generating and Tuning “Raisin Pudding”-Type Nanozymes with Multiple Enzyme-like Activities: Toward Online Electrochemical Detection of 3,4-Dihydroxyphenylacetic Acid in Living Brains. *ACS Appl. Mater. Interfaces* **2020**, *12*, 29631–29640. [[CrossRef](#)] [[PubMed](#)]
127. Li, Y.; Yu, C.; Yang, B.; Liu, Z.; Xia, P.; Wang, Q. Target-catalyzed hairpin assembly and metal-organic frameworks mediated nonenzymatic co-reaction for multiple signal amplification detection of miR-122 in human serum. *Biosens. Bioelectron.* **2018**, *102*, 307–315. [[CrossRef](#)]
128. Ren, G.; Dong, F.; Zhao, Z.; Li, K.; Lin, Y. Structure Defect Tuning of Metal–Organic Frameworks as a Nanozyme Regulatory Strategy for Selective Online Electrochemical Analysis of Uric Acid. *ACS Appl. Mater. Interfaces* **2021**, *13*, 52987–52997. [[CrossRef](#)]
129. Zhao, Y.; Zhang, H.; Li, Y.; Yu, X.; Cai, Y.; Sha, X.; Wang, S.; Zhan, Z.; Xu, J.; Liu, L. AI powered electrochemical multi-component detection of insulin and glucose in serum. *Biosens. Bioelectron.* **2021**, *186*, 113291. [[CrossRef](#)]
130. Giordano, G.F.; Freitas, V.M.S.; Schleder, G.R.; Santhiago, M.; Gobbi, A.L.; Lima, R.S. Bifunctional metal meshes acting as a semipermeable membrane and electrode for sensitive electrochemical determination of volatile compounds. *ACS Appl. Mater. Interfaces* **2021**, *13*, 35914–35923. [[CrossRef](#)]
131. Zhu, X.; Lin, L.; Wu, R.; Zhu, Y.; Sheng, Y.; Nie, P.; Liu, P.; Xu, L.; Wen, Y. Portable wireless intelligent sensing of ultra-trace phyto regulator α -naphthalene acetic acid using self-assembled phosphorene/Ti₃C₂MXene nanohybrid with high ambient stability on laser induced porous graphene as nanozyme flexible electrode. *Biosens. Bioelectron.* **2021**, *179*, 113062. [[CrossRef](#)] [[PubMed](#)]
132. Schroeder, V.; Evans, E.D.; Wu, Y.C.M.; Voll, C.C.A.; McDonald, B.R.; Savagatrup, S.; Swager, T.M. Chemiresistive sensor array and machine learning classification of food. *ACS Sens.* **2019**, *4*, 2101–2108. [[CrossRef](#)] [[PubMed](#)]
133. Dykstra, G.; Reynolds, B.; Smith, R.; Zhou, K.; Liu, Y. Electropolymerized molecularly imprinted polymer synthesis guided by an integrated data-driven framework for cortisol detection. *ACS Appl. Mater. Interfaces* **2022**, *14*, 25972–25983. [[CrossRef](#)] [[PubMed](#)]
134. Paul, A.; Dhamu, V.N.; Muthukumar, S.; Prasad, S. E.P.A.S.S: Electroanalytical pillbox assessment sensor system, a case study using metformin hydrochloride. *Anal. Chem.* **2022**, *94*, 10617–10625. [[CrossRef](#)]
135. Kalasin, S.; Sangnuang, P.; Surareungchai, W. Lab-on-Eyeglasses to monitor kidneys and strengthen vulnerable populations in pandemics: Machine learning in predicting serum creatinine using tear creatinine. *Anal. Chem.* **2021**, *93*, 10661–10671. [[CrossRef](#)]
136. Wang, B.; Li, W.; Lu, Q.; Zhang, Y.; Yu, H.; Huang, L.; Wang, T.; Liang, X.; Liu, F.; Liu, F.; et al. Machine learning-assisted development of sensitive electrode materials for mixed potential-type NO₂ gas sensors. *ACS Appl. Mater. Interfaces* **2021**, *13*, 50121–50131. [[CrossRef](#)]

Disclaimer/Publisher’s Note: The statements, opinions and data contained in all publications are solely those of the individual author(s) and contributor(s) and not of MDPI and/or the editor(s). MDPI and/or the editor(s) disclaim responsibility for any injury to people or property resulting from any ideas, methods, instructions or products referred to in the content.